SINGLE-TRACK VEHICLE MODELING AND CONTROL

DAVID J.N. LIMEBEER and ROBIN S. SHARP

Bicycles, Motorcycles, and Models

The potential of human-powered transportation was recognized over 300 years ago. Human-propelled vehicles, in contrast with those that utilized wind power, horse power, or steam power, could run on that most readily available of all resources: willpower. The first step beyond four-wheeled horse-drawn vehicles was to make one axle cranked and to allow the rider to drive the axle either directly or through a system of cranks and levers. These vehicular contraptions [1], [2] were so cumbersome that the next generation of machines was fundamentally different and based on only two wheels.

The first such development came in 1817 when the German inventor Baron Karl von Drais, inspired by the idea of skating without ice, invented the running machine, or draisine [3]. On 12 January 1818, von Drais received his first patent from the state of Baden; a French patent was awarded a month later. The draisine shown in Figure 1 features a small stuffed rest, on which the rider's arms are

1066-033X/06/$20.00©2006IEEE

laid, to maintain his or her balance. The front wheel was steerable. To popularize his machine, von Drais traveled to France in October 1818, where a local newspaper praised his skillful handling of the draisine as well as the grace and speed with which it descended a hill. The reporter also noted that the baron's legs had "plenty to do" when he tried to mount his vehicle on muddy ground. Despite a mixed reception, the draisine enjoyed a short period of European popularity. In late 1818, the draisine moved to England, where Denis Johnson improved its design and began manufacturing the hobby horse. Despite the public's enduring desire for rider-propelled transportation, the draisine was too flawed to survive as a viable contender; basic impediments were the absence of drive and braking capabilities.

Although the history of the invention of the pedal-drive bicycle is riven with controversy [2], traditional credit for introducing the first pedal-driven two wheeler, in approximately 1840, goes to the Scotsman Kirkpatrick Macmillan [1]. Another account has it that pedals were introduced in 1861 by the French coach builder Pierre Michaux when a customer brought a draisine into his shop for repairs and Michaux instructed his son Ernest to affix pedals to the broken draisine. In September 1894, a memorial was dedicated in honor of the Michaux machine. Shown in Figure 2, this vehicle weighed an unwieldy 60 pounds and was known as the velocipede, or bone shaker. This nickname derives from the fact that the velocipede's construction, in combination with the cobblestone roads of the day, made for an extremely uncomfortable ride. Although velocipedomania only lasted about three years (1868–1870), the popularity of the machine is evidenced by the large number of surviving examples. A common complaint among velocipedists was that the front wheel caught their legs when cornering. As a result, machines with centrally hinged frames and rear-steering were tested but with little success [4].

FIGURE 1 The draisine, or running, machine. This vehicle, which was first built in Germany in 1816, is early in a long line of inventions leading to the contemporary bicycle. (Reproduced with permission of the Bicycle Museum of America, New Bremen, Ohio.)

FIGURE 2 Velocipede by Pierre Michaux et Cie of Paris, France circa 1869. In the wake of the draisine, the next major development in bicycle design was the velocipede, which was developed in France and achieved its greatest popularity in the late 1860s. The velocipede marks the beginning of a continuous line of developments leading to the modern bicycle. Its most significant improvement over the draisine was the addition of cranks and pedals to the front wheel. Different types of (not very effective) braking mechanisms were used, depending on the manufacturer. In the case of the velocipede shown, the small spoon brake on the rear wheel is connected to the handlebar and is engaged by a simple twisting motion. The wheels are wooden wagon wheels with steel tires. (Reproduced with permission of the Canada Science and Technology Museum, Ottawa, Canada.)

Speed soon became an obsession, and the velocipede suffered from its bulk, its harsh ride, and a poor gear ratio to the driven wheel. In 1870, the first light all-metal machine appeared. The "ordinary" or penny farthing had its pedals attached directly to a large front wheel, which provided improved gearing (see Figure 3). Indeed, custom front wheels were available that were as large as one's leg length would allow. Solid rubber tires and the long spokes of the large front wheel provided a smoother ride than its predecessors. This machine, which was the first to be called a "bicycle," was the world's first single-track vehicle to employ the center-steering head that is still in use today. These bicycles enjoyed great popularity among young men of means during their hey-day in the 1880s. Thanks to its adjustable crank and several other new mechanisms, the penny farthing racked up record speeds of about 7 m/s. As is often said, pride comes before a fall. The high center of gravity and forward position of the rider made the penny farthing difficult to mount and dismount as well as dynamically challenging to ride. In the event that the front wheel hit a stone or rut in the road, the entire machine rotated forward about its front axle, and the rider, with his legs trapped under the handlebars, was dropped unceremoniously on his head. Thus the term "taking a header" came into being.

Another important invention was the pneumatic tire introduced by John Boyd Dunlop in 1899. The new tires substantially improved the cushioning of the

ride and the achievable top speed. Dunlop sold the marketing rights to his pneumatic tire to the Irish financier Harvey Du Cros, and together they launched the Pneumatic Tyre Company, which supplied inflatable tires to the British bicycle industry. To make their tires less puncture prone, they introduced a stout canvas lining to the inner surface of the tire carcass while thickening the inner tube [2].

A myriad of other inventions and developments have made the bicycle what it is today. For bicycles using wheels of equal size, key innovations include chain and sprocket drive systems, lightweight stiff steel frames, caliper brakes, sprung seats, front and rear suspension systems, free-running drive hubs, and multispeed Derailleur gear trains [1], [5].

A comprehensive and scholarly account of the history of the bicycle can be found in [2]. Archibald Sharp's book [1] gives a detailed account of the early history of the bicycle and a thorough account of bicycle design as it was understood in the 19th century. Archibald Sharp was an instructor in engineering design at the Central Technical College of South Kensington (now Imperial College). Although Sharp's dynamical analysis of the bicycle is only at a high school physics course level, it is sure footed and of real interest to the professional engineer who aspires to a proper appreciation of bicycle dynamics and design.

FIGURE 3 Penny farthing, or ordinary. This bicycle is believed to have been manufactured by Thos Humber of Beeston, Nottinghamshire, England, circa 1882. The braking limitations of this vehicle's layout are obvious! (Reproduced with permission of the Glynn Stockdale Collection, Knutsford, England.)

FIGURE 4 Sylvester Roper steam motorcycle. This vehicle is powered by a two-cylinder steam engine that uses connecting rods fixed directly to the rear wheel. (Reproduced with permission of the Smithsonian Museum, Washington, D.C.)

EARLY POWERED MACHINES

If one considers a wooden frame with two wheels and a steam engine a "motorcycle," then the first one was probably American. In 1867, Sylvester Howard Roper demonstrated a motorcycle (Figure 4) at fairs and circuses in the eastern United States. His machine was powered by a charcoal-fired, two-cylinder engine, whose connecting rods drove a crank on the rear wheel. The chassis of the Roper steam velocipede was based on the bone-shaker bicycle.

Gottlieb Daimler is considered by many to be the inventor of the first true motorcycle, or motor bicycle, since his machine was the first to employ an internal combustion engine. After training as a gunsmith, Daimler became an engineer and worked in Britain, France, and Belgium before being appointed technical director of the gasoline engine company founded by Nikolaus Otto. After a dispute with Otto in 1882, Daimler and Wilhelm Maybach set up their own company. Daimler and Maybach concentrated on producing the first lightweight, high-speed gasoline-fueled engine. They eventually developed an engine with a surface-mounted carburetor that vaporized the petrol and mixed it with air; this Otto-cycle engine produced a fraction of a kilowatt. In 1885 Daimler and Maybach combined a Daimler engine with a bicycle, creating a machine with iron-banded, wooden-spoked front and rear wheels as well as a pair of smaller spring-loaded outrigger wheels (see Figure 5).

The first successful production motorcycle was the Hildebrand and Wolfmueller, which was patented in Munich in 1894 (see Figure 6). The engine of this vehicle was a 1,428-cc water-cooled, four-stroke parallel twin, which was mounted low on the frame with cylinders in a fore-and-aft configuration; this machine produced less than 2 kW and had a top speed of approximately 10 m/s. As with the Roper steamer, the engine's connecting rods were coupled directly to a crank on the rear axle. The Hildebrand and Wolfmueller, which was manufactured in France under the name Petrolette, remained in production until 1897.

Albert Marquis de Dion and his engineering partner Georges Bouton began producing self-propelled steam vehicles in 1882. A patent for a single-cylinder gasoline engine was filed in 1890, and production began five years later. The De Dion Bouton engine, which was a small, lightweight, high-rpm four-stroke "single," used battery-and-coil ignition, thereby doing away with the troublesome hot-tube ignition system. The engine had a bore of 50

mm and a stroke of 70 mm, giving rise to a swept volume of 138 cc. De Dion Bouton also used this fractional kilowatt engine, which was widely copied by others including the Indian and Harley-Davidson companies in the United States, in road-going tricycles. The De Dion Bouton engine is arguably the forerunner of all motorcycle engines.

Testosterone being what it is, the first motorcycle race probably occurred when two motorcyclists came across each other while out for a spin. From that moment on, the eternal question in motorcycling circles became: "How do I make my machine faster?" As one would imagine, the quest for speed has many dimensions, and it would take us too far afield to try to analyze these issues in detail. In the context of modeling and control, it is apparent that the desire for increased speed as well as the quest to more fully utilize machine capability, requires high-fidelity models, control theory, and formal dynamic analysis. One also needs to replace the fractional kilowatt Otto-cycle engine used by Daimler with a much more powerful one. Indeed, modern high-performance two- and four-stroke motorcycle engines can rotate at almost 20,000 rpm and produce over 150 kW. In combination with advanced materials, modern tires, sophisticated suspension systems, stiff and light frames, and the latest in brakes, fuels, and lubricants, these powerful engines have led to Grand Prix machines with straight-line speeds of approximately 100 m/s. Figure 7 shows Ducati's Desmosedici GP5 racing motorcycle currently raced by Loris Capirossi.

The parameters and geometric layout that characterize the dynamic behavior of modern motorcycles can vary widely. Ducati's Desmosedici racing machine has a steep steering axis and a short wheelbase. These features produce the fast steering and the agile maneuvering required for racing. The chopper motorcycle, such as the one shown in Figure 8, is at the other extreme, having a heavily raked steering axis and a long wheelbase. "Chopped" machines are not just aesthetically different; they also have distinctive handling properties that are typified by a very stable feel at high straight-line speeds as compared with more conventional machine geometries. However, as with many other modifications, this stable feel is accompanied by less attractive dynamic features such as a heavy feel to the front end and poor responsiveness at slow speeds and in corners.

Web sites and virtual museums dedicated to bicycles and motorcycles are ubiquitous. See, for example, [6]–[10] for bicycles and [11]–[15] for motorcycles.

BICYCLE MODELING AND CONTROL

Background

From a mathematical modeling perspective, single-track vehicles are multibody systems; these vehicles include bicycles, motorcycles, and motor scooters, all of which have broadly similar dynamic properties. One of the earliest

FIGURE 5 Daimler petrol-powered motorcycle. Gottlieb Daimler, who later teamed up with Karl Benz to form the Daimler-Benz Corporation, is credited with building the first motorcycle in 1885. (Reproduced with permission of DaimlerChrysler AG, Stuttgart, Germany.)

FIGURE 6 Hildebrand and Wolfmueller motorcycle. This machine, patented in 1894, was the first successful production motorcycle. (Reproduced with permission of the Deutsches Zweirad- und NSU-Museum, Neckarsulm, Germany.)

FIGURE 7 Loris Capirossi riding the Ducati Desmosedici GP5. Ducati Corse's MotoGP racing motorcycle is powered by a V-4 four-stroke 989-cc engine. The vehicle has a maximum output power of approximately 161 kW at 16,000 rpm. The corresponding top speed is in excess of 90 m/s. (Reproduced with permission of Ducati Corse, Bologna, Italy.)

FIGURE 8 "Manhattan" designed and built by Vic Jefford of Destiny Cycles. Manhattan received the Best in Show award at the 2005 Bulldog Bash held at the Shakespeare County Raceway, Warwickshire, England. Choppers, such as the one featured, are motorcycles that have been radically customized to meet a particular taste. The name *chopper* came into being after the Second World War when returning GIs bought up war surplus motorcycles and literally chopped off the components they did not want. According to the taste and purse of the owner, high handle bars, stretched and heavily raked front forks, aftermarket exhaust pipes, and chrome components are added. Custom-built choppers have extreme steering-geometric features that have a significant impact on the machine's handling properties. These features include a low head angle, long forks, a long trail, and a long wheelbase. The extreme steering geometry of Manhattan includes a steering head angle of 56°! (Reproduced with the permission of Destiny Cycles, Kirkbymoorside, Yorkshire, England.)

attempts to analyze the dynamics of bicycles appeared in 1869 as a sequence of five short articles [16]. These papers use arguments based on an heuristic inverted-pendulum-type model to study balancing, steering, and propulsion. Although rear-wheel steering was also contemplated, it was concluded that "A bicycle, then, with the steering wheel behind, may possibly be balanced by a very skillful rider as a feat of dexterity; but it is not suitable for ordinary use in practice." These papers are interesting from a historical perspective but are of little technical value today.

The first substantial contribution to the theoretical bicycle literature was Whipple's seminal 1899 paper [17], which is arguably as contributory as anything that followed it; see "Francis John Welsh Whipple." This remarkable paper contains, for the first time, a set of nonlinear differential equations that describe the general motion of a bicycle and rider. The possibility of the rider applying a steering torque input by using a torsional steering spring is also considered. Since appropriate computing facilities were not available at the time, Whipple's general nonlinear equations could not be solved and consequently were not pursued beyond simply deriving and reporting them. Instead, Whipple studied a set of linear differential equations that correspond to small motions about a straight-running trim condition at a given constant speed.

Whipple's model, which is essentially the model considered in the "Basic Bicycle Model" section, consists of two frames—the rear frame and the front frame—which are hinged together along an inclined steering-head assembly. The front and rear wheels are attached to the front and rear frames, respectively, and are free to rotate relative to them. The rider is described as an inert mass that is rigidly attached to the rear frame. The rear frame is free to roll and translate in the ground plane. Each wheel is assumed to be thin and thus touches the ground at a single ground-contact point. The wheels, which are also assumed to be nonslipping, are modeled by holonomic constraints in the normal (vertical) direction and by nonholonomic constraints [18] in the longitudinal and lateral directions. There is no aerodynamic drag representation, no frame flexibility, and no suspension system; the rear frame is assumed to move at a constant speed. Since Whipple's linear straight-running model is fourth order, the corresponding characteristic polynomial is a quartic. The stability implications associated with this equation are deduced using the Routh criteria.

Concurrent with Whipple's work, and apparently independently of it, Carvallo [19] derived the equations of motion for a free-steering bicycle linearized around a straight-running equilibrium condition. Klein and Sommerfeld [20] also derived equations of motion for a straight-running bicycle. Their slightly simplified model (as compared with that of Whipple) lumps all of the front-wheel assembly mass into the front wheel. The main purpose of their study was to determine the effect of the gyroscopic moment due to the front wheel on the machine's free-steering stability. While this moment does indeed stabilize the free-steering bicycle over a range of speeds, this effect is of only minor importance because the rider can easily replace the stabilizing influence of the front wheel's gyroscopic precession with low-bandwidth rider control action [21].

An early attempt to introduce side-slipping and force-generating tires into the bicycle literature appears in [22]. Other classical contributions to the theory of bicycle dynamics include [23] and [24]. The last of these references, in its original 1967 version, appears to contain the first analysis of the stability of the straight-running bicycle fitted with pneumatic tires; several different tire models are considered. Reviews of the bicycle literature from a dynamic modeling perspective can be found in [25] and [26]. The bicycle literature is comprehensively reviewed from a control theory perspective in [27], which also describes interesting bicycle-related experiments.

Some important and complementary applied work has been conducted in the context of bicycle dynamics. An attempt to build an unridable bicycle (URB) is described in [21]. One of the URBs described had the gyroscopic moment of the front wheel canceled by another that was counterrotating. The cancellation of the front wheel's gyroscopic moment made little difference to the machine's apparent stability and handling qualities. It was also found that this riderless bicycle was unstable, an outcome that had been predicted

theoretically in [20]. Three other URBs described in [21] include various modifications to their steering geometry. These modifications include changes in the front-wheel radius and the magnitude and sign of the fork offset. Experimental investigations of bicycle dynamics have also been conducted in the context of teaching [28].

Francis John Welsh Whipple

Francis John Welsh Whipple (see Figure A) was born on 17 March 1876. He was educated at the Merchant Taylors' School and was subsequently admitted to Trinity College, Cambridge, in 1894. His university career was brilliant, and he received his B.A. degree in mathematics in 1897 as second wrangler. (*Wrangler* is a term that refers to Cambridge honors graduates receiving a first-class degree in the mathematics tripos; the senior wrangler is the first on the list of such graduates.) In 1898, he graduated in the first class in Part II of the mathematics tripos. Whipple received his M.A. degree in 1901 and an Sc.D. in 1929. In 1899, he returned to the Merchant Taylors' School as mathematics master, a post he held until 1914. He then moved to the Meteorological Office as superintendent of instruments.

Upon his death in 1768, Robert Smith, master of Trinity College, Cambridge and previously Plumian professor of astronomy, left a bequest establishing two annual prizes for proficiency in mathematics and natural philosophy to be awarded to junior bachelors of arts. The prizes have been awarded every year since, except for 1917 when there were no candidates. Throughout its existence, the competition has played a significant role by enabling graduates considering an academic career, and the majority of prize winners have gone on to become professional mathematicians or physicists. In 1883, the Smith Prizes ceased to be awarded through examination and were given instead for the best two essays on a subject in mathematics or natural philosophy.

On 13 June 1899, the results of the Smith Prize competition were announced in the *Cambridge University Reporter* [84]. Whipple did not win the prize, but it was written: "The adjudicators are of the opinion that the essay by F.J.W. Whipple, B.A., of Trinity College, 'On the stability of motion of a bicycle,' is worthy of honorable mention."

The main results of this essay depend on the work of another Cambridge mathematician, Edward John Routh, who received his B.A. degree in mathematics from Cambridge in 1854. He was senior wrangler in the mathematical tripos examinations, while James Clerk Maxwell placed second. In 1854, Maxwell and Routh shared the Smith Prize; George Gabriel Stokes set the examination paper for the prize, which included the first statement of Stokes' theorem.

Figure B, which was generated directly from a quartic equation given in Whipple's paper, shows the dynamic properties of a forward- and reverse-running bicycle as a function of speed. Whipple found the parameters by experiment on a particular machine. It is surely the case that Whipple would have loved to have seen this figure—derived from the remarkable work of a young man of 23, working almost 100 years before the widespread availability of MATLAB!

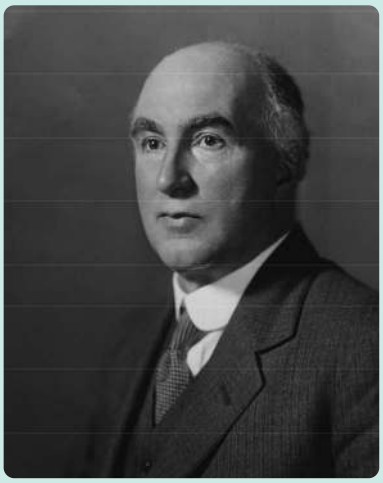

FIGURE A Francis John Welsh Whipple by Elliot and Fry. Francis Whipple was assistant director of the Meteorological Office and Superintendent of the Kew Observatory from 1925–1939. He served as president of the Royal Meteorological Society from 1936–1938. Apart from his seminal work on bicycle dynamics, he made many other contributions to knowledge, including identities for generalized hypergeometric functions, several of which have subsequently become known as Whipple's identities and transformations. He devised his meteorological slide rule in 1927. He introduced a theory of the hair hygrometer and analyzed phenomena related to the great Siberian meteor. (Picture reproduced with the permission of the National Portrait Gallery, London.)

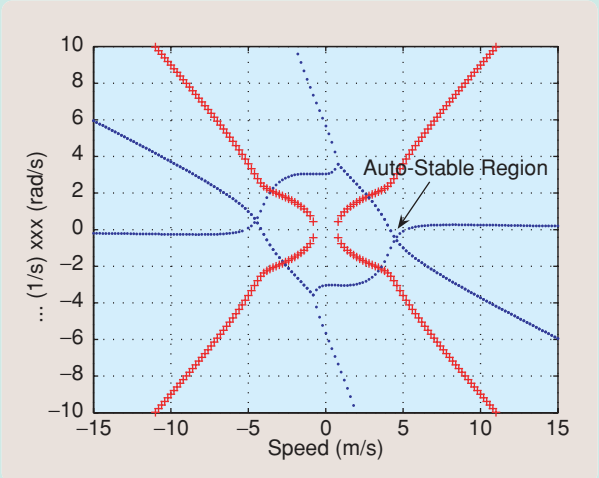

FIGURE B Stability properties of the Whipple bicycle. Real and imaginary parts of the eigenvalues of the straight-running Whipple bicycle model as functions of speed. Plot generated using equation (XXVIII) in [17].

Point-Mass Models

Bicycles and motorcycles are now established as nonlinear systems that are worthy of study by control theorists and vehicle dynamicists alike. In most cases, control-theoretic work is conducted using simple models, which are special cases of the model introduced by Whipple [17]. An early example of such a model can be found in [29] (see equations (e) and (j) on pages 240 and 241, respectively, of [29]). These equations describe the dynamics of a point-mass bicycle model of the type shown in Figure 9; [29] presents both linear and nonlinear models. Another early example of a simple nonholonomic bicycle study in a control systems context can be found in [30], which gives a servo-related interpretation of the self-steer phenomenon. A more contemporary nonholonomic bicycle, which is essentially the same as that presented in [29], was introduced in [31] and [32]. This model is studied in [32] and [33] in the context of trajectory tracking. A model of this type is also examined in [27] in the context of the performance limitations associated with nonminimum phase zeros.

The coordinates of the rear-wheel ground-contact point of the inverted pendulum bicycle model illustrated in Figure 9 are given in an inertial reference frame O-xyz. The Society of Automotive Engineers (SAE) sign convention is used: x-forward, y-right, and z-down for axis systems and a right-hand-rule for angular displacements. The roll angle φ is around the x-axis, while the yaw angle ψ is around the z-axis. The steer angle δ is measured between the front frame and the rear frame.

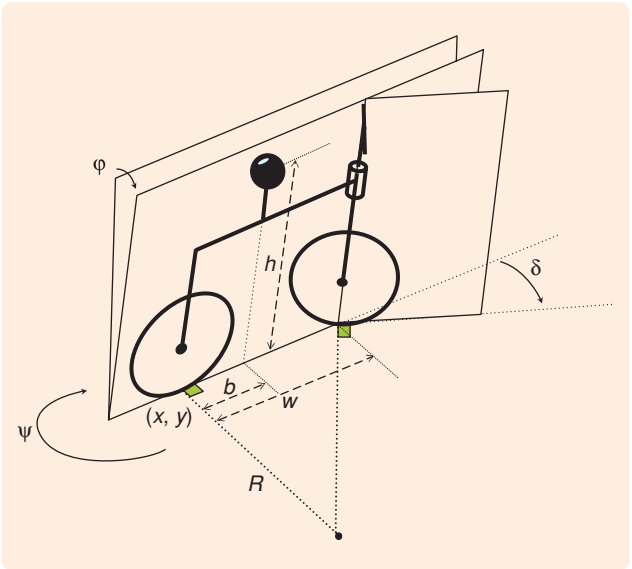

FIGURE 9 Inverted pendulum bicycle model. Schematic diagram of an elementary nonholonomic bicycle with steer δ, roll φ, and yaw ψ degrees of freedom. The machine's mass is located at a single point h above the ground and b in front of the rear-wheel ground-contact point. The wheelbase is denoted w. Both wheels are assumed to be massless and to make point contact with the ground. Both ground-contact points remain stationary during maneuvering as seen from the rear frame. The path curvature is $\sigma(t) = 1/R(t)$.

The vehicle's entire mass m is concentrated at its mass center, which is located at a distance h above the ground and distance b in front of the rear-wheel ground-contact point. The acceleration due to gravity is denoted g, and w is the wheelbase. The motion of the bicycle is assumed to be constrained so that there is no side slipping of the vehicle's tires and thus the rolling is nonholonomic. The kinematics of the planar motion are described by

$$\dot{x} = v\cos\psi, \tag{1}$$

$$\dot{y} = v\sin\psi, \tag{2}$$

$$\dot{\psi} = \frac{v\tan\delta}{w\cos\varphi}, \tag{3}$$

where v is the forward speed.

The roll dynamics of the bicycle correspond to those of an inverted pendulum with an acceleration influence applied at the vehicle's base and are given by

$$h\ddot{\varphi} = g\sin\varphi - \Big[(1 - h\sigma\sin\varphi)\sigma v^2 + b\left(\ddot{\psi} + \dot{v}\left(\sigma - \frac{\dot{\varphi}}{v}\right)\right)\Big]\cos\varphi, \tag{4}$$

where the vehicle's velocity and yaw rate are linked by the curvature σ satisfying $v\sigma = \dot{\psi}$. Using (3) to replace $\ddot{\psi}$ in (4) by the steer angle yields

$$h\ddot{\varphi} = g\sin\varphi - \tan\delta\left(\frac{v^2}{w} + \frac{b\dot{v}}{w} + \tan\varphi\left(\frac{vb}{w}\dot{\varphi} - \frac{hv^2}{w^2}\tan\delta\right)\right) - \frac{bv\dot{\delta}}{w\cos^2\delta}. \tag{5}$$

Equation (5) represents a simple nonholonomic bicycle with the control inputs δ and v. The equation can be linearized about a constant-speed, straight-running condition to obtain the simple small-perturbation linear model

$$\ddot{\varphi} = \frac{g}{h}\varphi - \frac{v^2}{hw}\delta - \frac{bv}{wh}\dot{\delta}. \tag{6}$$

In the constant-speed case, the only input is the steer angle.

Taking Laplace transforms yields the single-input, single-output transfer function

$$H_{\varphi\delta}(s) = -\frac{bv}{wh}\frac{s + v/b}{s^2 - g/h}, \tag{7}$$

which has the speed-dependent gain $(-bv)/(wh)$, a speed-dependent zero at $-v/b$, and fixed poles at $\pm\sqrt{g/h}$; the unstable pole $\sqrt{g/h}$ corresponds to an inverted-pendulum-type capsize mode. The zero $-v/b$, which is in the left-half plane under forward-running conditions, moves through the origin into the right-half plane as the speed is reduced and then reversed in sign. Under backward-running

conditions, the right-half plane zero, which for some speeds comes into close proximity to the right-half plane pole, is associated with the control difficulties found in rear-steering bicycles [34].

Basic Bicycle Model

We use AUTOSIM [35] models, which are derivatives of that given in [26], to illustrate the important dynamic properties of the bicycle. As with Whipple's model, the models we consider here consist of two frames and two wheels.

Figure 10 shows the axis systems and geometric layout of the bicycle model studied here. The bicycle's rear frame assembly has a rigidly attached rider and a rear wheel that is free to rotate relative to the rear frame. The front frame, which comprises the front fork and handlebar assembly, has a front wheel that is free to rotate relative to the front frame. The front and rear frames are attached using a hinge that defines the steering axis. In the reference configuration, all four bodies are symmetric relative to the bicycle midplane. As with Whipple's model, the nonslipping road wheels are modeled by holonomic constraints in the normal (vertical) direction and by nonholonomic constraints in the longitudinal and lateral directions. There is no aerodynamic drag, no frame flexibility, no propulsion, and no rider control. Under these assumptions, the bicycle model has three degrees of freedom—the roll angle φ of the rear frame, the steering angle δ, and the angle of

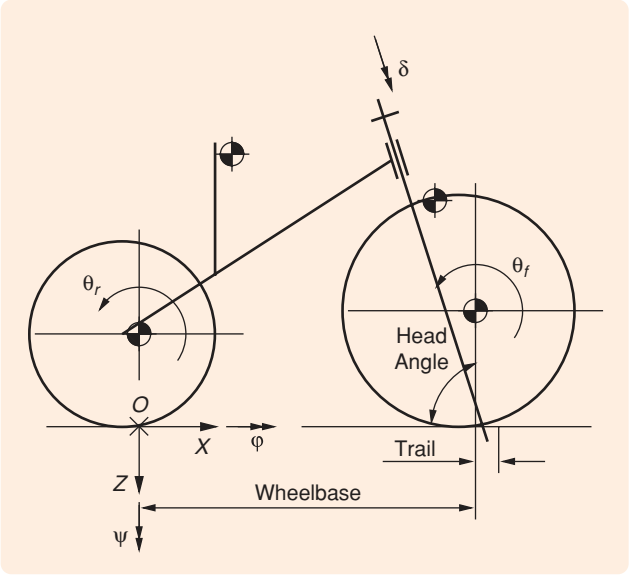

FIGURE 10 Basic bicycle model with its degrees of freedom. The model comprises two frames pinned together along an inclined steering head. The rider is included as part of the rear frame. Each wheel is assumed to contact the road at a single point.

TABLE 1 Parameters of the benchmark bicycle. These parameters are used to populate the AUTOSIM model described in [26] and its derivatives. The inertia matrices are referred to body-fixed axis systems that have their origins at the body's mass center. These body-fixed axes are aligned with the inertial reference frame $0 - xyz$ when the machine is in its nominal state.

Parameters	Symbol	Value
Wheel base	w	1.02 m
Trail	t	0.08 m
Head angle	α	arctan(3)
Gravity	g	9.81 N/kg
Forward speed	v	variable m/s
Rear wheel (rw)		
Radius	R_{rw}	0.3 m
Mass	m_{rw}	2 kg
Mass moments of inertia	(A_{xx}, A_{yy}, A_{zz})	(0.06,0.12,0.06) kg-m^2
Rear frame (rf)		
Position center of mass	(x_{rf}, y_{rf}, z_{rf})	(0.3,0.0,-0.9) m
Mass	m_{rf}	85 kg
Mass moments of inertia	$\begin{bmatrix} B_{xx} & 0 & B_{xz} \\ & B_{yy} & 0 \\ \text{sym} & & B_{zz} \end{bmatrix}$	$\begin{bmatrix} 9.2 & 0 & 2.4 \\ & 11 & 0 \\ \text{sym} & & 2.8 \end{bmatrix}$ kg-m^2
Front frame (ff)		
Position center of mass	(x_{ff}, y_{ff}, z_{ff})	(0.9,0.0,-0.7) m
Mass	m_{ff}	4 kg
Mass moments of inertia	$\begin{bmatrix} C_{xx} & 0 & C_{xz} \\ & C_{yy} & 0 \\ \text{sym} & & C_{zz} \end{bmatrix}$	$\begin{bmatrix} 0.0546 & 0 & -0.0162 \\ & 0.06 & 0 \\ \text{sym} & & 0.0114 \end{bmatrix}$ kg-m^2
Front wheel (fw)		
Radius	R_{fw}	0.35 m
Mass	m_{fw}	3 kg
Mass moments of inertia	(D_{xx}, D_{yy}, D_{zz})	(0.14,0.28,0.14) kg-m^2

rotation θ_r of the rear wheel relative to the rear frame. The steering angle δ represents the rotation of the front frame with respect to the rear frame about the steering axis.

The dimensions and mechanical properties of the benchmark model are taken from [26] and presented in Table 1. All inertia parameters use the relevant body-mass centers as the origins for body-fixed axes. The axis directions are then chosen to align with the inertial O-xyz axes when the bicycle is in its nominal state, as shown in Figure 10. Products of inertia A_{xz}, B_{xz} and so on are defined as $-\int\int m(x,z)xzdxdz$.

As derived in [17] and explained in [26], the linearized equations of motion of the constant-speed, straight-running nonholonomic bicycle, expressed in terms of the generalized coordinates $q = (\varphi, \delta)^T$, have the form

$$M\ddot{q} + vC\dot{q} + (v^2K_2 + K_0)q = m_{\text{ext}}\,, \tag{8}$$

where M is the mass matrix, the damping matrix C is multiplied by the forward speed v, and the stiffness matrix has a constant part K_0 and a part K_2 that is multiplied by the square of the forward speed. The right-hand side m_{ext} contains the externally applied moments. The first component of m_{ext} is the roll moment m_φ that is applied to the rear frame. The second component is the action-reaction steering moment m_δ that is applied between the front frame and the rear frame. This torque could be applied by the rider or by a steering damper. In the uncontrolled bicycle, both external moments are zero. This model, together with nonslipping thin tires and the parameter values of Table 1, constitute the basic bicycle model.

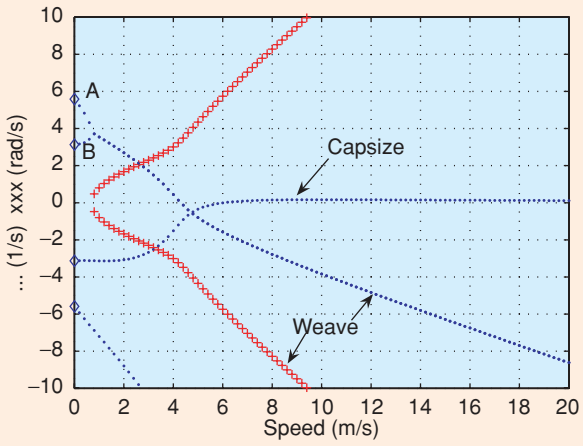

FIGURE 11 Basic bicycle straight-running stability properties. The real and imaginary parts of the eigenvalues of the straight-running basic bicycle model are plotted as functions of speed. The (blue) dotted lines correspond to the real part of the eigenvalues, while the (red) crosses show the imaginary parts for the weave mode. The weave mode eigenvalue stabilizes at $v_w = 4.3$ m/s, while the capsize mode becomes unstable at $v_c = 6.1$ m/s giving the interval of auto-stability $v_c \geq v \geq v_w$.

To study (8) in the frequency domain, we introduce the matrix-valued polynomial

$$P(s,v) = s^2M + svC + (v^2K_2 + K_0)\,, \tag{9}$$

which is quadratic in both the forward speed v and in the Laplace variable s. The associated dynamic equation is

$$\begin{bmatrix} P_{11}(s) & P_{12}(s,v) \\ P_{21}(s,v) & P_{22}(s,v) \end{bmatrix} \begin{bmatrix} \varphi(s) \\ \delta(s) \end{bmatrix} = \begin{bmatrix} m_\varphi(s) \\ m_\delta(s) \end{bmatrix}, \tag{10}$$

where P_{11} is independent of v. When studying stability, the roots of the speed-dependent quartic equation

$$\det(P(s,v)) = 0 \tag{11}$$

need to be analyzed using the Routh criteria or found by numerical methods. Figure 11 shows the loci of the roots of (11) as functions of the forward speed. The basic bicycle model has two important modes—the weave and capsize modes. The weave mode begins at zero speed with the two real, positive eigenvalues marked A and B in Figure 11. The eigenvector components corresponding to the A-mode eigenvalue have a steer-to-roll ratio of −37; the negative sign means that as the bicycle rolls to the left, for instance, the steering rotates to the right. This behavior shows that the motion associated with the A mode is dominated by the front frame diverging toward full lock as the machine rolls over under gravity. Because real tires make distributed contact with the ground, a real bicycle cannot be expected to behave in exact accordance with this prediction. The eigenvector components corresponding to the B-mode eigenvalue have a steer-to-roll ratio of −0.57. The associated motion involves the rear frame toppling over, or capsizing, like an unconstrained inverted pendulum to the left, for instance, while the steering assembly rotates relative to the rear frame to the right with 0.57 of the roll angle.

Note that the term "capsize" is used in two different contexts. The static and very-low-speed capsizing of the bicycle is associated with the point B in Figure 11 and the associated nearby locus. The locus marked capsize in Figure 11 is associated with the higher-speed unstable toppling over of the machine. This mode crosses the stability boundary and becomes unstable when the matrix $v^2K_2 + K_0$ in (8) is singular.

As the machine speed builds up from zero, the two unstable real modes combine at approximately 0.6 m/s to produce the oscillatory fish-tailing weave mode. The basic bicycle model predicts that the weave mode frequency is approximately proportional to speed above 0.6 m/s. In contrast, the capsize mode is a nonoscillatory motion, which when unstable corresponds to the riderless bicycle slowly toppling over at speeds above 6.057 m/s. From the perspective of bicycle riders and designers, this mode is unimportant because it is easy for the

rider to stabilize it using a low-bandwidth steering control torque. In practice, the capsize mode can also be stabilized using appropriately phased rider body motions, as is evident from hands-free riding.

In the recent measurement program [36], an instrumented bicycle was used to validate the basic bicycle model described in [17] and [26]. The measurement data show close agreement with the model in the 3–6 m/s speed range; the weave mode frequency and damping agreement is noteworthy. The transition of the weave mode from stable to unstable speed ranges is also accurately predicted by the basic bicycle model. These measurements lend credibility to the idea that tire and frame compliance effects can be neglected for benign maneuvering in the 0–6 m/s range.

Special Cases

Several special cases of the basic bicycle model are now used to illustrate some of the key features of bicycle behavior. These cases include the machine's basic inverted-pendulum-like characteristics, as well as its complex steering and self-stabilizing features. Some of these features are the result of carefully considered design compromises.

Locked Steering Model

The dynamically simple locked steering case is considered first. If the steering degree of freedom is removed, the steering angle $\delta(s)$ must be set to zero in (10), and consequently the roll freedom is described by

$$\begin{aligned} m_\varphi(s) &= P_{11}(s)\varphi(s) \\ &= (s^2 T_{xx} + g m_t z_t)\varphi(s)\,. \end{aligned} \tag{12}$$

The roots of $P_{11}(s)$ are given by

$$p_\pm = \pm\sqrt{\frac{g m_t z_t}{T_{xx}}}\,, \tag{13}$$

where m_t is the total mass of the bicycle and rider, z_t is the height of the combined mass center above the ground, and T_{xx} is the roll moment of inertia of the entire machine around the wheelbase ground line. In the case of the basic bicycle model, $p_\pm = \pm 3.1348$. For the point-mass, Timoshenko-Young model, $z_t = h$ and $T_{xx} = mh^2$ and so $p_\pm = \pm\sqrt{g/h}$.

Since the steering freedom is removed, the A mode (see Figure 11) does not appear. The vehicle's inability to steer also means that the weave mode disappears. Instead, the machine's dynamics are fully determined by the speed-independent, whole-vehicle capsize (inverted pendulum) mode seen at point B in Figure 11 and given by (13). Not surprisingly, motorcycles have a tendency to capsize at low speeds if the once-common friction pad steering damper is tightened down far enough to lock the steering system; see [37].

Point-Mass Model with Trail and Inclined Steering

Interesting connections can now be made between the Timoshenko-Young-type point-mass model and the more complex basic bicycle model. To forge these links, we set to zero the masses of the wheels and the front frame, as well as all the inertia terms in (10). The trail and steering inclination angle are left unaltered.

We first reconcile (7) and the first row of equation (10), which is

$$\varphi(s) = \frac{-P_{12}(s, v)}{P_{11}(s, v)}\delta(s), \tag{14}$$

when the roll torque is $m_\varphi(s) = 0$. As in [26], we denote the trail by t and the steering inclination angle as measured from the vertical by λ. Direct calculation gives

$$H_{\varphi\delta}(s, v) = \frac{-P_{12}}{P_{11}}(s, v) \tag{15}$$

$$= -\frac{\cos(\lambda)(tbs^2 + sv(b + t) + v^2 - gtb/h)}{wh(s^2 - g/h)}\,. \tag{16}$$

Equation (16) reduces to (7) when λ and t are set to zero. It follows from (10) and $m_\varphi = 0$ that

$$H_{\varphi m_\delta}(s, v) = \frac{-P_{12}}{\det(P)}(s, v)\,, \tag{17}$$

which reduces to

$$H_{\varphi m_\delta}(s, v) = \frac{w(tbs^2 + sv(t + b) + v^2 - gtb/h)}{mtbg(s^2 - g/h)(hw\sin(\lambda) - tb\cos(\lambda))} \tag{18}$$

under the present assumptions. In contrast to the analysis given in [27], (18) shows that the poles of $H_{\varphi m_\delta}(s, v)$ are fixed at $\pm\sqrt{g/h}$ and that the steering inclination and trail do not alone account for the self-stabilization phenomenon in bicycles.

We now compute $H_{\delta m_\delta}(s, v)$ as

$$\begin{aligned} H_{\delta m_\delta}(s, v) &= \frac{P_{11}}{\det P}(s, v) \\ &= \frac{hw^2}{mtbg\cos(\lambda)(hw\sin(\lambda) - tb\cos(\lambda))}\,, \end{aligned} \tag{19}$$

which is a constant. Equation (19) shows that in a point-mass specialization of the Whipple model, the steer angle δ and the steering torque m_δ are related by a virtual spring whose stiffness depends on the trail and steering axis inclination. Physically, this static dependence means that the steer angle of the point-mass bicycle responds instantaneously to steering torque inputs. It also follows from (19) that this response is unbounded in the case of a zero-trail ($t = 0$) machine [29] because in this case the connecting spring has a stiffness of zero.

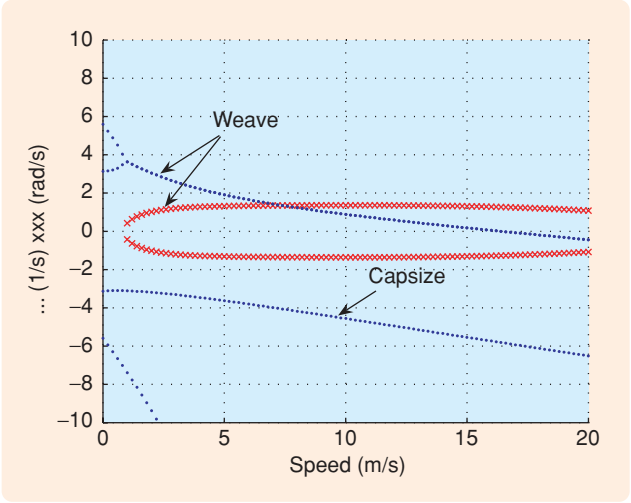

FIGURE 12 Bicycle straight-running stability properties. This plot shows the real and imaginary parts of the eigenvalues of the straight-running basic bicycle model with the gyroscopic moment associated with the front road wheel removed by setting $D_{yy} = 0$. The (blue) dotted lines correspond to the real parts of the eigenvalues, while the (red) pluses show the imaginary parts for the weave mode.

No Trail, Steering Inclination, or Front-Frame Mass Offset

We now remove the basic bicycle's trail (by setting $t = 0$), the inclination of the steering system (by setting $\lambda = 0$), and the front-frame mass offset by setting $x_{\rm ff} = w$. This case is helpful in identifying some of the key dynamical features of the steering process. The first row in (10) relates the roll angle to the steer angle when $m_\varphi = 0$, and shows how the inverted pendulum system is forced by the steer angle together with $\dot{\delta}$ and $\ddot{\delta}$. The second row of (10) is

$$(s^2 C_{xz} - s\Omega_{\rm fw} D_{yy})\varphi(s) + \{s^2(C_{zz} + D_{zz}) + s(C_{zz} + D_{zz})v/w)\}\delta(s) = m_\delta(s), \quad (20)$$

where $\Omega_{\rm fw}(s)$ is the angular velocity of the front wheel. The $\varphi(s)$ term in (20), which is the self-steering term, shows how the roll angle influences the steer angle. The first component of the self-steering expression is a product of inertia, which generates a steering moment from the roll acceleration. The second self-steering term represents a gyroscopic steering moment generated by the roll rate. The expression for P_{22} in (20) relates the steering torque to the steering angle through the steered system inertia and a physically obscure speed-proportionate damper, apparently coming from the rear-wheel ground-contact model.

No Trail or Steering Inclination

We now modify the previous special case by including front-frame mass offset effects ($x_{\rm ff} \neq w$). As before, the first row of (10), which relates the roll angle to the steering angle when $m_\varphi = 0$, represents steer angle forcing of the inverted pendulum dynamics. The second row of (10) in this case is shown in (21), found at the bottom of the page. The quadratic self-steering term in (21) contains a new term involving $x_{\rm ff} - w$ that comes from the fact that the front-frame mass is no longer on the steering axis, implying an increase in the effective xz-plane product of inertia of the front frame. The constant self-steering term in (21) represents a mass-offset-related gravitational moment, which is proportional to the roll angle. The steering mass offset also increases the moment of inertia of the steering system, enhances the steering damping, and introduces a new speed-dependent stiffness term.

By comparing (20) and (21), it is suggested that the bicycle equations become too complicated to express in terms of the original data set when trail and steering inclination influences are included. Indeed, when these elaborations are introduced, it is necessary to resort to the use of intermediate variables and numerical analysis procedures [26]. In the case of state-of-the-art motorcycle models, the equations of motion are so complex that they can only be realistically derived and checked using computer-assisted multibody modeling tools.

Gyroscopic Effects

Gyroscopic precession is a favorite topic of conversation in bar-room discussions among motorcyclists. While it is not surprising that lay people have difficulty understanding these effects, inconsistencies also appear in the technical literature on single-track vehicle behavior. The experimental evidence is a good place to begin the process of understanding gyroscopic influences. Experimental bicycles whose gyroscopic influences are canceled through the inclusion of counterrotating wheels have been designed and built [21]. Other machines have had their gyroscopic influences exaggerated through the use of a high-moment-of-inertia front wheel [27]. In these cases, the bicycles were found to be easily ridable. As with the stabilization of the capsize mode by the rider, the precession-canceled bicycle appears to represent little more than a simple low-bandwidth challenge to the rider. As noted in [21], in connection with his precession-canceled bicycle, "... Its 'feel' was a bit strange, a fact I attributed to the increased moment of inertia about the front forks, but it did not tax my (average) riding skill even at low speed ...". It is also noted in [21] that

$$\left\{s^2(C_{xz} + m_{\rm ff} z_{\rm ff}(w - x_{\rm ff})) - s\Omega_{\rm fw} D_{yy} + g m_{\rm ff}(w - x_{\rm ff})\right\}\varphi(s) +$$
$$\left\{s^2(m_{\rm ff}(w - x_{\rm ff})^2 + C_{zz} + D_{zz}) + sv(C_{zz} + D_{zz} - m_{\rm ff} x_{\rm ff}(w - x_{\rm ff}))/w + v^2 m_{\rm ff}(w - x_{\rm ff})/w\right\}\delta(s) = m_\delta(s). \quad (21)$$

the precession-canceled bicycle has no autostable speed range, thereby verifying by experiment the findings reported in [20]. When trying to ride this particular bicycle without hands, however, the rider could only just keep it upright because the vehicle seemed to lack balance and responsiveness.

In their theoretical work, Klein and Sommerfeld [20] studied a Whipple-like quartic characteristic equation using the Routh criteria. While the basic bicycle model has a stable range of speeds, which Klein and Sommerfeld called the interval of autostability, this model with the spin inertia of the front wheel set to zero is unstable up to a speed of 16.4 m/s. This degraded stability can be seen in Figure 12, where the capsize mode remains stable with the damping increasing with speed; due to its stability, the capsize nomenclature may seem inappropriate in this case. In contrast, the weave mode is unstable for speeds below 16.4 m/s, and the imaginary part is never greater than 1.8 rad/s. Klein and Sommerfeld attribute the stabilizing effect of front-wheel precession to a self steering effect; as soon as a bicycle with spinning wheels begins to roll, the resulting gyroscopic moment due to the $s\Omega_{\mathrm{fw}}D_{yy}$ term in (20) causes the bicycle to steer in the direction of the fall. The front contact point, consequently, rolls towards a position below the mass center.

The Klein and Sommerfeld finding might leave the impression that gyroscopic effects are essential to auto-stabilization. However, it is shown in [38] that bicycles without trail or gyroscopic effects can autostabilize at modest speeds by adopting extreme mass distributions, but the design choices necessary do not make for a practical machine.

A Feedback System Perspective

Basic Bicycle as a Feedback System

To study the control issues associated with bicycles, we use the second row of (10) to solve for $\delta(s)$, which yields

$$\delta(s) = \frac{-P_{21}(s, v)}{P_{22}(s, v)}\varphi(s) + \frac{1}{P_{22}(s, v)}m_\delta(s). \tag{22}$$

Equations (22) and (14) are shown diagrammatically in the feedback configuration given in Figure 13. Eliminating $\varphi(s)$ yields the closed-loop transfer function

$$H_{\delta m_\delta}(s, v) = \frac{P_{11}}{\det(P)}(s, v)\,. \tag{23}$$

In [27], (22) is simplified to

$$\delta(s) = k_1(v)m_\delta(s) + k_2(v)\varphi(s)\,, \tag{24}$$

in which the mass and damping terms are neglected. If the wheel and front frame masses, as well as all of the inertia terms, are set to zero, these velocity-dependent gains are given by

$$k_1(v) = \frac{w^2}{tmb\cos\lambda(v^2\cos\lambda - gw\sin\lambda)}, \tag{25}$$

$$k_2(v) = \frac{wg}{v^2\cos\lambda - wg\sin\lambda}. \tag{26}$$

Although this stiffness-only model represents the low-frequency behavior of the steering system, the approximation obscures some of the basic bicycle model's structure. The poles and zeros of $H_{\delta m_\delta}(s, v)$, as a function of speed, are shown in Figure 14. Except for the pair of speed-independent zeros, this diagram contains the same information

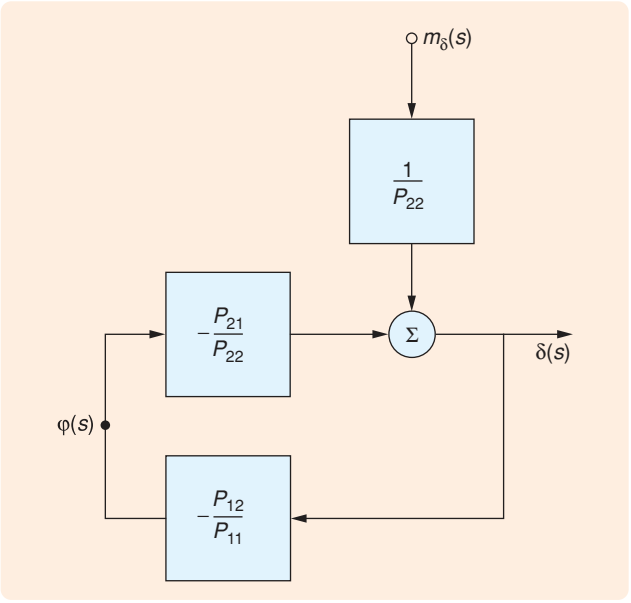

FIGURE 13 Block diagram of the *basic bicycle model* described in [26]. The steer torque applied to the handlebars is $m_\delta(s)$, $\varphi(s)$ is the roll angle, and $\delta(s)$ is the steer angle.

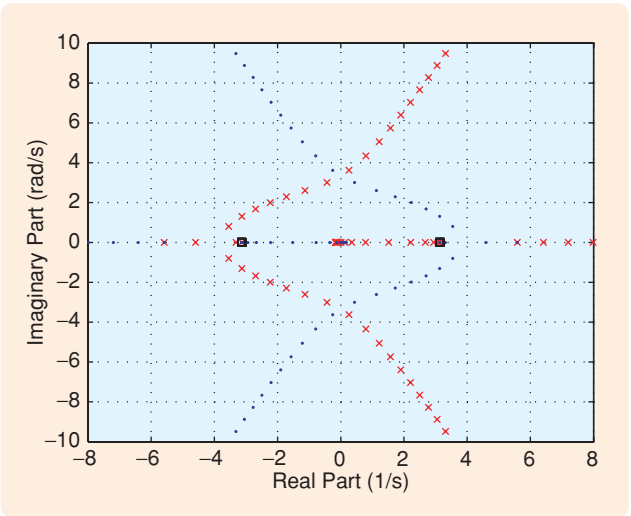

FIGURE 14 Poles and zeros of $H_{\delta m_\delta}(s, v)$ as functions of speed. The speed v is varied between ± 10 m/s. The poles are shown as blue dots for forward speeds and red crosses for reverse speeds. There are two speed-independent zeros shown as black squares at $\pm$ 3.135 1/s.

as that given in Figure 11. As the speed of the bicycle increases, the unstable poles associated with the static capsize modes coalesce to form the complex pole pair associated with the weave mode. The weave mode is stable for speeds above 4.3 m/s [26]. As the machine's speed increases further, it becomes unstable due to the dynamic capsize mode at 6.06 m/s.

The zeros of $H_{\delta m_\delta}(s, v)$, which derive from the roots of $P_{11}(s)$ as shown in (13) [see (23)], are associated with the speed-independent whole-vehicle capsize mode. The backward-running vehicle is seen to be unstable throughout the speed range, but this vehicle is designed for forward motion and, when running backwards, it has negative trail and a divergent caster action. See "Caster Shimmy" and note that the cubic terms of (38) and (39) are negative for negative speeds, indicating instability in this case.

A control theoretic explanation for the stabilization difficulties associated with backward-running bicycles centers on the positive zero fixed at $+\sqrt{gm_t z_t / T_{xx}}$, which is in close proximity to a right-half plane pole in certain speed ranges [34].

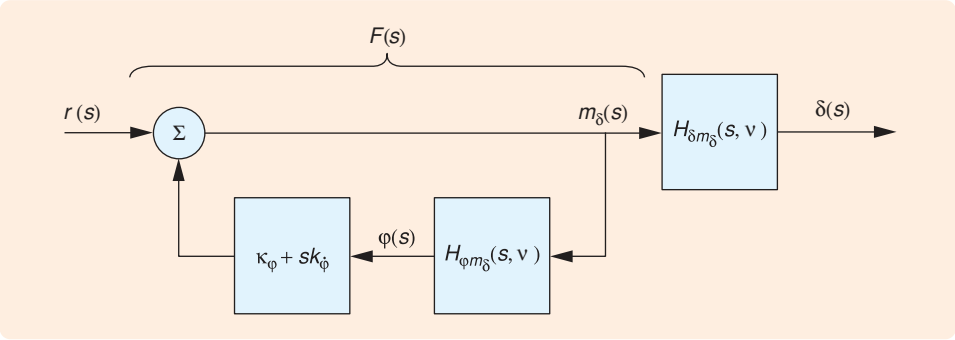

FIGURE 15 Steering torque prefilter $F(s)$ described in (29). This filter is an open-loop realization of the roll-angle-plus-roll-rate feedback law described in (28). As readers familiar with control systems are aware, open- and closed-loop systems can be represented in equivalent ways if there are no disturbances and no modeling uncertainties.

Steering

An appreciation of the subtle nature of bicycle steering goes back over 100 years. Archibald Sharp records [1, p. 222] "... to avoid an object it is often necessary to steer for a small fraction of a second towards it, then steer away from it; this is probably the most difficult operation the beginner has to master..." While perceptive, such historical accounts make no distinction between steering torque control and steering angle control. They do not highlight the role played by the machine speed, and timing estimates are based on subjective impressions rather than experimental measurement.

As Whipple [17] surmised, the rider's main control input is the steering torque. While in principle one can steer through leaning (by applying a roll moment to the rear frame), the resulting response is too sluggish to be practical in an emergency situation. The steer-torque-to-steer-angle response of the bicycle can be deduced from (23). Once the steer angle response is known, the small perturbation yaw rate response for the model described in [26] can be calculated using

$$\dot{\psi} = \frac{v \cos\lambda \delta}{w + t/\cos\lambda},$$

which corresponds to (3) for the Timoshenko-Young bicycle with small perturbation restrictions. In the case of small perturbations from straight running, (2) becomes

$$\dot{y} = v\psi.$$

It now follows that the transfer function linking the lateral displacement to the steer angle is

$$H_{y\delta}(s, v) = \frac{v^2 \cos\lambda}{s^2(w + t/\cos\lambda)} \tag{27}$$

and that the transfer function linking the lateral displacement to the steering torque is given by $H_{y\delta}(s, v)H_{\delta m_\delta}(s, v)$, with $H_{\delta m_\delta}(s, v)$ given in (23). This transfer function is used in the computation of responses to step steering torque inputs.

To study the basic bicycle model's steering response at different speeds, including those outside the autostable speed range, it is necessary to introduce stabilizing rider control. The rider can be emulated using the roll-angle plus roll-rate feedback law

$$m_\delta(s) = r(s) + (k_\varphi + sk_{\dot{\varphi}})\varphi(s), \tag{28}$$

in which $r(s)$ is a reference torque input and k_φ and $k_{\dot{\varphi}}$ are the roll and roll-rate feedback gains, respectively. This feedback law can be combined with (17) to obtain the open-loop stabilizing steer-torque prefilter

$$F(s) = \frac{\det(P(s, v))}{\det(P(s, v)) + (k_\varphi + sk_{\dot{\varphi}})P_{12}(s, v)k(s)}, \tag{29}$$

which maps the reference input $r(s)$ into the steering torque $m_\delta(s)$ as shown in Figure 15. In the autostable speed range, the stabilizing prefilter is not needed and $F(s)$ is set to unity in this case. The bicycle's steering behavior can now be studied at speeds below, within, and above the autostable speed range. Prior to maneuvering, the machine is in a constant-speed straight-running trim condition. For an example of each of the three cases, the filtered steering torque and the corresponding roll-angle

responses are shown in Figure 16, while the steer angle and lateral displacement responses are shown in Figure 17. In each case, the filter gains are chosen to be stabilizing and to achieve approximately the same steady-state roll angle; numerical gain values appear in the figure captions. The autostable case is considered first, because no stabilizing torque demand filtering is required. In this case, the clockwise (when viewed from above) unit-step steer torque demand is applied directly to the bicycle's steering system (see Figure 16). The machine initially steers to the right and the rear wheel ground-contact point starts moving to the right also (see Figure 17). Following the steer torque input, the bicycle immediately rolls to the left (see Figure 16) in preparation for a left-hand turn. After approximately 0.6 s, the steer angle sign reverses, while the rear-wheel ground-contact point begins moving to the left after approximately 1.2 s. The oscillations in the roll angle and steer angle responses have a frequency of about 0.64 Hz and are associated with the weave mode of the bicycle (see Figure 11). Therefore, to turn to the left, one must steer to the right so as the make the machine roll to the left. This property of the machine to apparently roll in the wrong direction is sometimes referred to as countersteering [39], [27], but an alternative interpretation is also possible, as seen below. The nonminimum phase behavior in the steer angle and lateral displacement responses is attributable to the right-half plane zero in $H_{\delta m_\delta}(s, v)$ given by the roots of $P_{11}(s) = 0$ and corresponding to the locked-steering whole-machine capsize mode as illustrated in (13). Toward the end of the simulation shown, the steer angle settles into an equilibrium condition, in which the bicycle turns left in a circle with a fixed negative roll angle. In relation to the nonminimum phase response in the lateral displacement behavior, the reader is reminded of the control difficulty that arises if one rides near to a curb or a drop [39]; to escape, one has to go initially closer to the edge. Body lean control is unusually useful in such circumstances.

At speeds below the autostable range, a stabilizing steering-torque prefilter must be utilized to prevent the machine from toppling over. In the low-speed (3.7 m/s) case, the steer torque illustrated in Figure 16 is the unit-step response of the prefilter, which is the steer torque required to establish a steady turn. The output of the prefilter is unidirectional apart from the superimposed weave-frequency oscillation required to stabilize the bicycle's unstable weave mode. In the case considered here, the steady-state steer torque is more than twice the autostable unit-valued reference torque required to bring the machine to a steady-state roll angle of approximately −0.65 rad. To damp the weave oscillations in the roll and

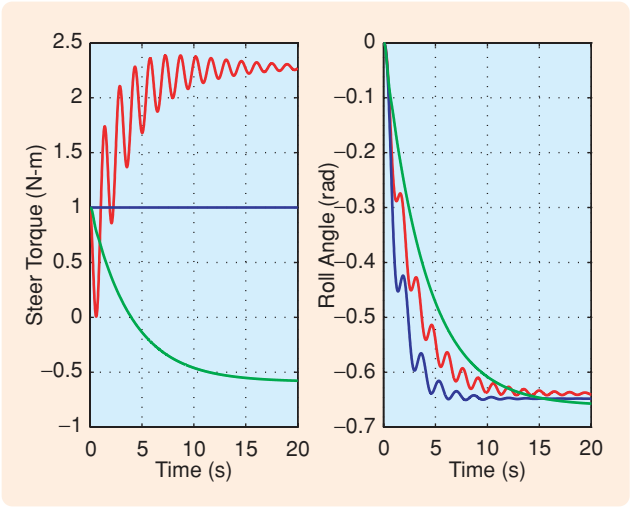

FIGURE 16 Step responses of the prefilter and the roll angle of the basic bicycle model. The steering torque and roll angle response at the autostable speed of 4.6 m/s are shown in blue; the prefilter gains are $k_\varphi = 0$ and $k_{\dot\varphi} = 0$. The low-speed 3.7 m/s case, which is below the autostable speed range, is shown in red; the stabilizing prefilter gains are $k_\varphi = -2$ and $k_{\dot\varphi} = 3$. The high-speed 8.0-m/s case, which is above the autostable speed range, is shown in green; the stabilizing prefilter gains are $k_\varphi = 2.4$ and $k_{\dot\varphi} = 0.02$. In each case, a clockwise steering moment (viewed from above) causes the machine to roll to the left. This tendency of the machine to apparently roll "in the wrong direction" is sometimes referred to as countersteering. In the high-speed case (green curves), the steering torque is positive initially and then negative. This need to steer in one direction to initiate the turning roll response, and then to later apply an opposite steering torque that stabilizes the roll angle, is a high-speed phenomenon.

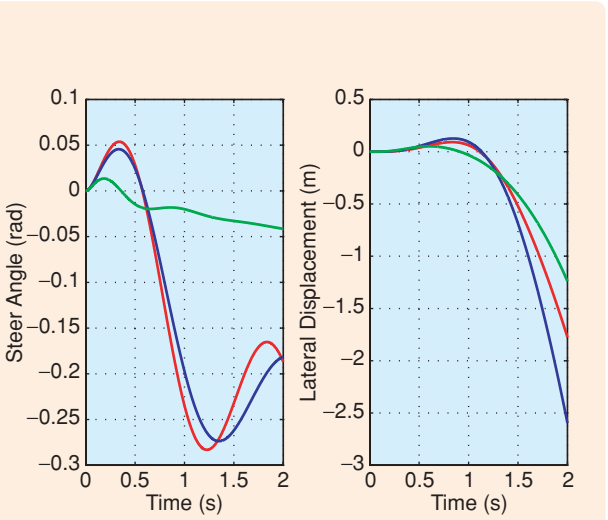

FIGURE 17 Response of the simple bicycle model to a steering moment command. The steer angle and the rear-wheel ground-contact point displacement responses at the autostable speed of 4.6 m/s are shown in blue; the prefilter gains are $k_\varphi = 0$ and $k_{\dot\varphi} = 0$. The responses at a speed of 3.7 m/s, which is below the autostable speed range, are shown in red; the stabilizing prefilter gains are $k_\varphi = -2$ and $k_{\dot\varphi} = 3$. The responses at a speed of 8.0 m/s, which is above the auto-stable speed range, are shown in green; the stabilizing prefilter gains are $k_\varphi = 2.4$ and $k_{\dot\varphi} = 0.02$. The steer angle and lateral displacement responses show the influence of the right-half-plane zero of $P_{11}(s)$. This zero is associated with the unstable whole-vehicle capsize mode. See point *A* in Figure 11 and (13).

steer angle responses, the torque demand filter, which mimics the rider, introduces weave-frequency fluctuations into the steering torque. The steer angle and lateral displacement responses are similar to those obtained in the autostable case.

If the trim speed is increased to the upper limit of the autostable range (in this case 6.1 m/s; see Figure 11), then the steady-state steering torque required to maintain an equilibrium steady-state turn falls to zero; this response is due to the singularity of the stiffness matrix $v^2K_2 + K_0$ at this speed. At speeds above the autostable range, stabilizing rider intervention is again required. As before, in response to a positive steer torque input, the steer angle and lateral displacement initially follow the steer torque (see Figure 17). At the same time the machine rolls to the left (see Figure 16). Moments later, one observes the nonminimum phase response in the steer angle and the lateral displacement responses. The interesting variation in this case is in the steering torque behavior. This torque is initially positive and results in the machine rolling to the left. However, if this roll behavior were left unchecked, the bicycle would topple over, and so to avoid the problem the steer torque immediately reduces and then changes sign after approximately 4 s. The steer torque then approaches a steady-state value of -0.6 N-m to stabilize the roll angle and maintain the counterclockwise turn. This need to steer in one direction to initiate the turning roll angle response, and then to later apply an opposite steering torque that stabilizes the roll angle is a high-speed phenomenon, providing the alternative interpretation of countersteering mentioned earlier. Countersteering in the first sense is always present, while in the second sense it is a high-speed phenomenon only. It is interesting to observe that the prefilter enforces this type of countersteering for all stabilizing values of k_φ and $k_{\dot\varphi}$. First note that the direct feedthrough (infinite frequency) gain of $F(s)$ is unity. Since k_φ and $k_{\dot\varphi}$ are stabilizing, all of the denominator coefficients of $F(s)$ have the same sign as do all of the numerator terms in the autostable speed range. As the speed passes from the autostable range, $\det(v^2K_2 + K_0)$ changes sign, as does the constant coefficient in the numerator of $F(s)$. Therefore, at speeds above the autostable range, $F(s)$ has a negative steady-state gain, thereby enforcing the sign reversal in the steering torque as observed in Figure 16.

We conclude this section by associating the basic bicycle model's nonminimum phase response (in the steer angle) with its self-steering characteristics. To do this, consider removing the basic bicycle's ability to self-steer by setting $\alpha = \pi/2$, $t = 0$, $C_{xz} = 0$, $D_{yy} = 0$, and $x_{\rm ff} = w$. With these changes in place, it is easy to see from (20) that $P_{21}(s, v) = 0$. This identity means that

$$H_{\delta m_\delta} = \frac{1}{P_{22}(s, v)} = \frac{1}{s(C_{zz} + D_{zz})(s + v/w)}, \tag{30}$$

which is clearly minimum phase and represents the response one would expect when applying a torque to a pure inertia with a damper to ground.

Pneumatic Tires, Flexible Frames, and Wobble

A modified version of the basic bicycle model is now considered in which a flexible frame and side-slipping tires are included. The flexibility of the frame is modeled by including a single rotational degree of freedom located between the steering head and the rear frame. In the model studied here, the twist axis associated with the frame flexibility freedom is in the plane of symmetry and perpendicular to the steering axis, and the associated motion is restrained by a parallel spring-damper combination. In this modified model, the nonholonomic lateral ground contact constraints are replaced by (31) and (32); see "Tire Modeling." These equations represent tires that produce lateral forces in response to sideslip and camber, with time lags dictated by the speed and the tires' relaxation lengths. The tire and frame flexibility data used in this study are given in Table 2; two representative values for the frame stiffness K_P and frame damping C_P are included. The higher values of K_P and C_P are associated with a stiff frame, while the lower values correspond to a flexible frame.

First, we examine the influence of frame compliance alone on the system eigenvalues, which can be seen in Figure 18. The dotted curve corresponds to the rigid frame that was studied in Figure 11 and is included here for reference purposes. The cross- and circle-symbol loci correspond to the stiff and flexible frames, respectively. The first important observation is that the model predicts wobble when frame compliance is included; see "Wobble." In the case of the flexible frame, the damping of the wobble mode reaches a minimum at about 10 m/s and the mode has a resonant frequency of approximately 6 Hz. In the case of the stiff frame, the wobble mode's resonant frequency increases, while its damping factor decreases, with increasing speed. Figure 18 also illustrates the impact of frame flexibility on the damping of the weave mode. At low speeds, frame flexibility has no impact on the characteristics of the weave mode. At intermediate and high speeds, the weave-mode damping is

TABLE 2 Bicycle tire and frame flexibility parameters. Tire parameters include relaxation lengths and cornering- and camber-stiffness coefficients. The frame flexibility is described in terms of stiffness and damping coefficients. All of the parameter values are given in SI units.

Parameters	Value
σ_f, σ_r	0.1, 0.1
C_{fs}, C_{rs}	14.325, 14.325
C_{fc}, C_{rc}	1.0, 1.0
$K_P^{\rm low}$, $K_P^{\rm high}$	2,000, 10,000
$C_P^{\rm low}$, $C_P^{\rm high}$	20, 50

Tire Modeling

Classical bicycle models, such as those developed by Whipple [17], and Timoshenko and Young [29], describe the wheel-road contact as a constraint. The wheel descriptions involve rotational coordinates to specify the wheels' orientation and translational coordinates that describe the location of the road contact points. The rolling constraints connect these coordinates so that translational changes are linked to rotational ones. In the case of general motions, the rotational and translational coordinates cannot be linked algebraically, since this linkage is path dependent; thus the nomenclature "nonholonomic," or incomplete constraint [18, p. 14]. Instead, it is the rotational and translational velocities that are linked, and the rolling constraint renders the wheels' ground-contact points, or lines, absolutely stationary [24], [51], [52]. During motion, the wheel-ground contact points change with time, with each point on the wheel periphery coming into contact with the ground once per wheel revolution. In the case of the bicycle, it is illustrated that (nonholonomic) tire constraint modeling limits the fidelity of the vehicle model to low speeds only.

By 1950, the understanding of tire behavior had improved substantially, and it had become commonplace, although not universal, to regard the rolling wheel as a force producer rather than as a constraint on the vehicle's motion. With real tire behavior, the tread material at the ground contact "slips" relative to the road and so has a nonzero absolute velocity and the linkage between the wheels' rotational and translational velocities is lost. To model this behavior, it is necessary to introduce a slip-dependent tire force-generation mechanism.

To understand the underlying physical mechanisms underpinning tire behavior, it is necessary to analyze the interface between the elastic tire tread base and the ground. This distributed contact involves the tire carcass and the rubber tread material, which can be thought of as a set of bristles that join the carcass to the ground. Under dynamic conditions, these bristles move, as a continuous stream, into and out of the ground-contact region. Under free-rolling conditions, in common with the nonholonomic rolling model, the tread-base material is stationary; consequently, the bristles remain undeformed in bending as they pass through the contact region. When rolling resistance is neglected, no shear forces are developed. Free-rolling corresponds to zero slip, and, if a slip is developed, it has in general both longitudinal and lateral components [50], [51]. In contrast to the physical situation, tire models usually rely on the notion of a ground-contact point.

To assemble these ideas in a mathematical framework, let $\mathbf{v}_f$ denote the velocity of the tread base material at the ground contact point. In the case of no longitudinal slipping, $\mathbf{v}_f$ is perpendicular to the line of intersection between the wheel plane and the ground plane; the unit vector $\mathbf{i}$ lies along this line of intersection and the unit vector $\mathbf{j}$ is perpendicular to it. The velocity of a tread base point with respect to the wheel axle is given by $\mathbf{v}_{fr} = \omega_f R_f \mathbf{i}$, where ω_f is the wheel's spin velocity and R_f is the wheel radius. If we now associate with this ground contact point an "unspun" point, its velocity is $\mathbf{v}_f^{us} = \mathbf{v}_f + \mathbf{v}_{fr}$. The slip (for the front wheel) is defined as

$$\mathbf{s}_{\mathrm{sf}} = \frac{\mathbf{v}_f}{< \mathbf{v}_f^{us}, \mathbf{i} >},$$

where $< \cdot, \cdot >$ denotes the inner product. The slip is in the $\mathbf{j}$ direction in the case of no longitudinal slipping, as is assumed here. If the bristle bending stiffness is constant and the frictional coupling between the bristle tips and the ground is sufficient to prevent sliding, the lateral force developed is proportional to $\mathbf{s}_{\mathrm{sf}}$ and acts to oppose the slip.

When the rolling wheel is leaned over, then even with no slip, the tread base material becomes distorted from its unstressed state. This distortion leads to the development of a lateral force that is approximately equal to the normal tire load multiplied by the camber angle [51], [52]. If the tire is not working hard, the force due to camber simply superimposes on the force due to slip. The elemental lateral forces due to camber are distributed elliptically over the contact length, while those due to sustained slip increase with the longitudinal distance of the tire element from the point of first contact. As the sideslip increases, the no-sliding condition is increasingly challenged as the rear of the contact patch is approached. Thus, as the tire works harder in slip, sliding at the rear of the contact patch becomes more pronounced. Force saturation is reached once all the tire elements (bristles) in contact with the road begin to slide.

When the tire operates under transient conditions, following for example a step change in steering angle, the distortion of the tire tread material described above does not develop instantly. Instead, the distortion builds up in a manner that is linked to the distance covered from the time of application of the transient. For vehicle modeling purposes, a simple approximation of this behavior is to treat the dynamic force development process as a speed-dependent first-order lag. The characterizing parameter, called the relaxation length σ_f, is similar to a time constant except that it has units of length rather than time. The relaxation length is a tire characteristic that can be determined experimentally. The lateral force response of the tire due to steering, and therefore side slipping, is a dynamic response to the slip and camber angles of the tire, which is modeled as

$$\frac{\sigma_f}{|\mathbf{v}_f^{us}|}\dot{Y}_f + Y_f = Z_f(C_{\mathrm{fs}} s_{\mathrm{sf}} + C_{fc}\varphi_f), \tag{31}$$

where Z_f is the normal load on the front tire and φ_f is the front wheel's camber angle relative to the road (pavement). The force Y_f acts in the $\mathbf{j}$ direction and opposes the slip. The product $Z_f C_{fs}$ is the tire's cornering stiffness, while $Z_f C_{fc}$ is its camber stiffness. The sideforce associated with the rear tire is given analogously by

$$\frac{\sigma_r}{|\mathbf{v}_r^{us}|}\dot{Y}_r + Y_r = Z_r(C_{rs} s_{sr} + C_{rc}\varphi_r), \tag{32}$$

where each term has an interpretation that parallels that of the front wheel. Equations (31) and (32) are suitable only for small perturbation modeling.

Contemporary large perturbation tire models are based on magic formulas [51] and [53]–[55], which can mimic accurately measured tire force and moment data over a wide range of operating conditions.

Wobble

A phenomenon known variously as speedman's wobble, speed wobble, or death wobble is well known among cyclists [85] and [86]. As the name suggests, wobble is a steering oscillation belonging to a more general class—wheel shimmy. The oscillations are similar to those that occur with supermarket trolley wheels, aircraft nose wheels, and automobile steering systems. Documentation of this phenomenon in bicycles is sparse, but a survey [86] suggests that wobble at speeds between 4.5–9 m/s is unpleasant, while wobble at speeds between 9–14 m/s is dangerous. The survey [86] also suggests a wide spread of frequencies for the oscillations with the most common being between 3–6 Hz, somewhat less than for motorcycles. The rotation frequency of the front wheel is often close to the wobble frequency, so that forcing from wheel or tire nonuniformity may be an added influence. Although rough surfaces are reported as being likely to break the regularity of the wobble and thereby eliminate it, an initial event is normally needed to trigger the problem. Attempting to damp the vibrations by holding on tightly to the handlebars is ineffective, a result reproduced theoretically for a motorcycle [87]. The survey [86] recommends "pressing one or both legs against the frame, while applying the rear brake" as a helpful practical procedure, if a wobble should commence. The possibility of accelerating out of a wobble is mentioned, suggesting a worst-speed condition. The influences of loading are discussed with special emphasis on the loading of steering-frame-mounted panniers. Evidently, these influences are closely connected with the first term in each of (20) and (21), representing roll-acceleration-to-steer-torque feedback. Sloppy wheel or steering-head bearings and flexible wheels are described as contributory. Increasing the mechanical trail is considered stabilizing with respect to wobble, raising both the frequency and the worst-case speed, but is not necessarily advantageous overall.

In an important paper from a practical and experiential viewpoint, [37] implies that wobble was a common motorcycling phenomenon in the 1950s. Machines of the period were usually fitted with a rider-adjustable friction-pad steering damper. The idea was that the rider should make the damper effective for high-speed running and ineffective for lower speeds; see also [88]. Reference [37] offers the view that steering dampers should not be necessary for speeds under 45 m/s, indicating that, historically, wobble of motorcycles has been a high-speed problem. Reference [37] also points to the dangers of returning from high speed to low speed while forgetting to lower the preload on the steering damper. A friction lock on the steering system obliges a rider to use fixed (steering position) control, which we have earlier demonstrated to be difficult. The current status of motorcycle wobble analysis is covered in the "Motorcycle Modeling" section.

Wheel shimmy in general is discussed in detail in [51], where a whole chapter is devoted to the topic. Ensuring the stability of wheel shimmy modes in aircraft landing gear, automotive steering systems, and single-track vehicles is vital due to the potential violence of the oscillations in these contexts. An idea of how instability arises can be obtained by examining simple cases (see "Caster Shimmy"), but systems of practical importance are sufficiently complex to demand analysis by automated multibody modeling tools and numerical methods.

A simple system quite commonly employed to demonstrate wheel shimmy, both experimentally and theoretically [51], [89], is shown in Figure C. If the tire-to-ground contact is assumed to involve nonholonomic rolling, the characteristic equation of the system of Figure C is third order, and symbolic results for

compromised by the flexible frame, although this mode remains well damped. As is now demonstrated, the more realistic tire model has a strong impact on the predicted properties of both wobble and weave.

Figure 19 shows the influence of frame flexibility in combination with relaxed side-slipping tires. Again, the cross- and circle-symbol loci correspond to the stiff and flexible frames, respectively, while the dotted loci belong to the rigid-framed machine. As can be seen from this dotted locus, the introduction of side-slipping tires also produces a wobble mode, which is not a property of the basic bicycle. The predicted resonant frequency of the wobble mode varies from approximately 12.7–4.8 Hz, depending on the frame stiffness. Lower stiffnesses correspond to lower natural frequencies. With a rigid frame, the wobble damping is least at low and high speeds. With a compliant frame, the damping is least at an intermediate speed. The frame flexibility can be such that the resonant frequency aligns with the practical evidence. Frame flexibility modeling can also be used to align the wobble-mode damping with experimental measurement. Comparison with Figure 18 shows that the introduction of the side-slipping tire model causes a marked reduction in the wobble-mode frequency for the stiff-framed machine, while the impact of the side-slipping tires on the wobble mode of the flexible-framed machine is less marked. As with the flexible frame, side-slipping tires have little impact on the weave mode at very low speeds. However, as the speed increases, the relaxed side-slipping tires cause a significant reduction in the intermediate and high-speed weave-mode damping. By extension from measured motorcycle behavior, there is every reason to suspect that the accurate reproduction of bicycle weave- and wobble-mode behavior requires a model that includes both relaxed side-slipping tires and flexible frame representations.

MOTORCYCLE MODELING

Background

Several factors differentiate bicycles from motorcycles. A large motorcycle can weigh at least ten times as much as a

the conditions for stability are obtained in "Caster Shimmy." For higher levels of complexity, the system order is increased and analytical stability conditions become significantly more complex. In [51], a base set of parameter values is chosen, and stability boundaries are found numerically for systematic variations in speed v and mechanical trail e. The resulting stability boundaries are plotted in the (v, e) parameter space for several values of the lateral stiffness k of the king-pin mounting. The least oscillatory system is that having the highest stiffness, with the king-pin compliance contributing to the system behavior in much the same way tire lateral compliance contributes.

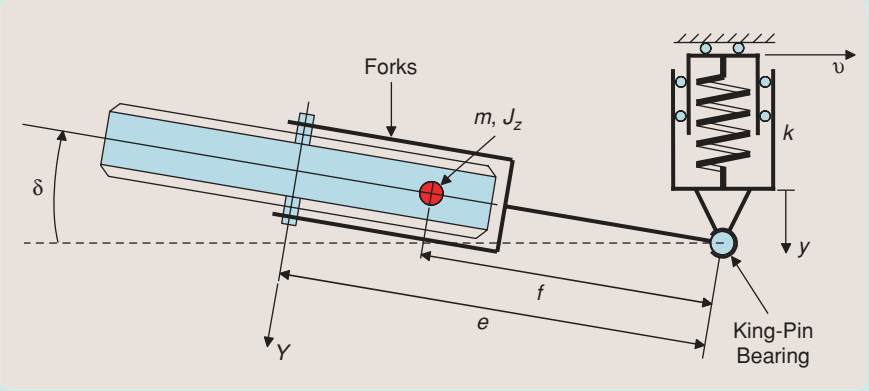

FIGURE C Plan view of a simple system capable of shimmy. This example is adapted from [51] and [89, pp. 333, 334, ex. 215 p. 414]. The wheel is axisymmetric and free to spin relative to the forks that support it; the wheel is deemed to have no spin inertia. The wheel has mechanical trail e and mass offset f with respect to the vertical king-pin bearing. The king-pin is free to translate laterally with displacement y from static equilibrium, while the whole assembly moves forward with constant speed v. The king-pin mounting has stiffness k, while the moving assembly has mass m. The steer angle is δ. The king-pin is assumed massless so that analysis deals with only one body; see "Caster Shimmy." The tire-ground contact can be treated on one of three different levels. First, pure (nonholonomic) rolling, implying no sideslip, can be assumed. Second, the tire may be allowed to sideslip thereby producing a proportionate and instantaneous side force. Third, the side force may be lagged relative to the sideslip by a first-order lag determined by the tire relaxation length; see "Tire Modeling."

Significant from the point of view of single-track vehicles, and aircraft nose-wheels, is the lateral compliance at the king-pin. If this compliance allows the assembly to rotate in roll about an axis well above the ground, as with a typical bicycle or motorcycle frame or aircraft fuselage, lateral motions of the wheel assembly are accompanied by camber changes. If, in addition, the wheel has spin inertia, gyroscopic effects have an important influence on the shimmy behavior. These effects are shown in [51] to create a second area of instability in the (v, e) space at higher speeds, which have a substantially different mode shape. The gyroscopic mode involves a higher ratio of lateral contact point velocity to steer velocity than occurs in situations in which a roll freedom is absent. This new phenomenon is called gyroscopic shimmy, and it is this shimmy variant that is particularly relevant to the single-track vehicle [40], [41], [47].

bicycle, and, consequently, in the case of a motorcycle, the rider's mass is a much smaller fraction of the overall rider-machine mass. A modern sports motorcycle can achieve top speeds of the order 100 m/s, while a modern sports bicycle might achieve a top speed of approximately 20 m/s. As a result of these large differences in speed, our understanding of the primary modes of bicycles must be extended to speeds that are usually irrelevant to bicycle behavioral studies. At high speeds, aerodynamic forces are important and need to be accounted for.

In his study of bicycles, Whipple [17] introduced a nondimensional approach to bicycle dynamic analysis, which is helpful when seeking to deduce the behavior of motorcycles from that of bicycles. The dimensionless model was obtained by representing each mass by $m = \alpha w$, where α is dimensionless and w has the units of mass (kilograms, for example) and each length quantity by $l = \beta b$, where β is dimensionless and b has the units of length (meters, for example). As a result, the moments and products of inertia are expressed as $J = \gamma w b^2$, where γ is also dimensionless. These changes of variable allowed Whipple to establish that the roots of the quartic characteristic equation, which represents the small perturbation behavior around a straight-running trim state, are independent of the mass units used. Therefore, for the nonholonomic bicycle model, increasing the masses and inertias of every body by the same factor makes no difference to the roots of the characteristic equation. In this restricted sense, a grown man riding a motorcycle is dynamically equivalent to a child riding a bicycle.

Whipple then showed that the characteristic equation $p(\lambda, v) = 0$ can be replaced with $\tilde{p}(\xi, \epsilon) = 0$ using a change of variables. In the first case, the speed v has units such as m/s, the characteristic equation has roots λ_i having the units of circular frequency (rad/s for example). The new variables: $\xi = \lambda b/v$ and $\epsilon = gb/v^2$, where g is the gravitational constant, are dimensionless as are the polynomial's coefficients. Therefore, all of the nondimensional single-track vehicles corresponding to $\tilde{p}(\xi, \epsilon) = 0$, where ϵ is a constant, have the same dynamical properties in terms of

Caster Shimmy

Caster wheel shimmy can occur in everyday equipment such as grocery trolleys, gurneys, and wheelchairs. These self-excited oscillations, which are energetically supported by the vehicle prime mover, are an important consideration in the design of aircraft landing gear and road vehicle suspension and steering systems. In the context of bicycles and motorcycles, this quantitative analysis is conducted by including the appropriate frame flexibility freedom and dynamic tire descriptions in the vehicle model. The details are covered in the "Pneumatic Tires, Flexible Frames, and Wobble" section.

By its nature, a caster involves a spinning wheel, a king-pin bearing, and a mechanical trail sufficient to provide a self-centering steering action. Our purpose here is to demonstrate how oscillatory instability can be predicted for the simple system of Figure C. In the case of small perturbations, the tire sideslip is

$$s = \delta + \frac{e\dot{\delta} - \dot{y}}{v}. \tag{33}$$

It follows from (31) that the resulting tire side force F is given by

$$\frac{\sigma}{v}\dot{Y} + Y = Cs, \tag{34}$$

in which C is the tire's cornering stiffness and σ is the relaxation length. The equations of motion for the swivel wheel assembly in Figure D are

$$m(\ddot{y} - f\ddot{\delta}) + ky - Y = 0 \tag{35}$$

and

$$J_z\ddot{\delta} + (e - f)Y + kyf = 0, \tag{36}$$

where J_z is the yaw-axis moment of inertia of the swiveled wheel assembly around the mass center. The characteristic polynomial associated with small motions in the system in Figure D is derived directly from (33)–(36). The resulting quintic polynomial is

$$\det\begin{bmatrix} ms^2 + k & -fms^2 & -1 \\ kf & s^2 J_z & e - f \\ Cs/v & -C(1 + (es)/v) & 1 + \sigma s/v \end{bmatrix}. \tag{37}$$

Two interesting special cases can be deduced from the general problem by making further simplifying assumptions. In the case of the nonholonomic wheel, the cornering stiffness becomes arbitrarily large for all values of σ, thereby preventing tire sideslip

$$\lim_{C\to\infty} \frac{\det[\cdot]}{kC} = \frac{(m(e-f)^2 + J_z)s^3}{kv} + \frac{m(e-f)s^2}{k} + \frac{e^2 s}{v} + e, \tag{38}$$

where $det[\cdot]$ comes from (37). It follows from (38) and the Routh criterion that shimmy occurs if $mf(e-f) \le J_z$, and in the case that $mf(e-f) = J_z$ the frequency of oscillation is $\omega = \sqrt{(ke)/(m(e-f))}$. These results show the role played by the steering system geometry, and the mass and inertia properties of the moving assembly in determining the stability, or otherwise, of the system. The king-pin stiffness influences the frequency of oscillation. The case of $mf(e-f) = J_z$ corresponds to a mass distribution in which the rolling contact is at the center of percussion relative to the kingpin. In this situation the rolling constraint has no influence on the sping force.

In the case of a rigid assembly

$$\lim_{k\to\infty} \frac{\det[\cdot]}{kC} = \frac{\sigma(f^2 m + J_z)s^3}{Cv} + \frac{(f^2 m + J_z)s^2}{C} + \frac{e^2 s}{v} + e. \tag{39}$$

It follows from (39) that shimmy occurs if $e \le \sigma$, and in the case that $e = \sigma$ the frequency of oscillation is $\omega = \sqrt{Ce/(f^2 m + J_z)}$. The tire properties dictate both conditions for the onset of shimmy and its frequency when it occurs. Interestingly, the tire relaxation length alone determines the onset, or otherwise, of shimmy, while the frequency of oscillation is dictated by the tire's cornering stiffness alone. The Pirelli company reports [90] on a tire tester that relies on this precise result. The test tire is mounted in a fork trailing a rigidly mounted king-pin bearing and runs against a spinning drum to represent movement along a road. Following an initial steer displacement of the wheel assembly, the exponentially decaying steering vibrations are recorded, and the decrement yields the tire relaxation length, while the frequency yields the cornering stiffness. Unlike the bicycle case, the shimmy frequency is independent of speed.

As discussed in the "Basic Bicycle Model" section, in connection with the zero-speed behavior, the simple caster does not in reality oscillate at vanishingly small speeds due to the distributed contact between the tire and the ground. The energy needed to increase the amplitude of unstable shimmy motions comes from the longitudinal force that sustains the forward speed of the king-pin. This longitudinal force is given by

$$F = m(\delta\ddot{y} + f\dot{\delta}^2) + \delta ky$$

for the small perturbation problem described in (33)–(36). In the case of a pure-rolling (nonholonomic) tire, $\dot{\delta}$ should be eliminated from the above equation using the zero-sideslip constraint $\dot{\delta} = (\dot{y} - v\delta)/e$.

ξ. The modal frequencies and decay/growth rates scale according to $e^{\lambda_i t}$ translating to $e^{(\xi_i v/b)t'}$, where t' is dimensionless. This analysis provides a method for predicting the properties of a family of machines from those of a single nondimensional vehicle. For example, if b is halved so as to represent a child's bicycle in this alternative length-scaling sense, then a simultaneous reduction of the speed by a factor of $\sqrt{2}$ leaves the roots of $\tilde{p}(\xi, \epsilon)$ unchanged. The

associated variation in the time domain response comes from λ_i translating to $\sqrt{2}\lambda_i$.

Whipple's scaling rules, in combination with observations, lead one to conclude that a viable motorcycle model 1) must be consistent with bicycle-like behavior at low speed, 2) must reproduce the autostability properties predicted by Whipple [17], 3) must reproduce the motorcycle's inclination to wobble at intermediate and high speeds, and 4) must reproduce the observed high-speed weave characteristics of modern high-performance motorcycles.

High-powered machines with stiff frames have a tendency to wobble at high speeds [40]–[42]; see "Tommy Smith's Wobble." A primary motivation for studying wobble and weave derives from the central role they play in performance and handling qualities. These modes are also associated with a technically challenging class of stability-related road accidents. Several high-profile accidents of this type are reviewed and explained in the recent literature [43]. Central to understanding the relevant phenomena is the ability to analyze the dynamics of motorcycles under cornering, where the in-plane and out-of-plane motions, which are decoupled in the straight-running situation, become interactive. Consequently, cornering models tend to be substantially more complex than their straight-running counterparts. This added complexity brings computer-assisted multibody modeling to the fore [42], [44], [45].

In the remainder of this article, we study several contributions, both theoretical and experimental, that have played key roles in bringing the motorcycle modeling art to its current state of maturity. Readers who are interested in the early literature are referred to the survey paper [46], which reviews theoretical and experimental progress up to the mid 1980s. That material focuses almost entirely on the straight-running case, which is now considered.

Straight-Running Motorcycle Models

An influential contribution to the theoretical analysis of the straight-running motorcycle is given in [47]. The model developed in [47] is intended to provide the minimum level of complexity required for predicting the capsize, weave, and wobble modes. This research is reminiscent of Whipple's analysis in terms of the assumptions concerning the rider and frame degrees of freedom. In contrast to Whipple, [47] treats the tires as force generators, which respond to both sideslip and camber; tire relaxation is included (see "Tire Modeling"), while aerodynamic effects are not.

A linearized model is used for the stability analysis through the eigenvalues of the dynamics matrix, which is a function of the vehicle's (constant) forward speed. Two cases are considered: one with the steering degree of freedom present, giving rise to the free-control analysis, and the other with the steering degree of freedom removed, giving rise to the fixed-control analysis. The free-control model predicts the existence of capsize, weave, and wobble modes. As with the bicycle, the capsize mode is a slowly divergent instability of the whole vehicle, which corresponds to the machine toppling over onto its side. This mode is relatively unimportant because it is easily (and subconsciously) controlled by the rider. As with the bicycle, weave is a low-frequency (2–3 Hz) oscillation of the whole vehicle involving roll, yaw, and steer motions, and is well damped at moderate speeds but becomes

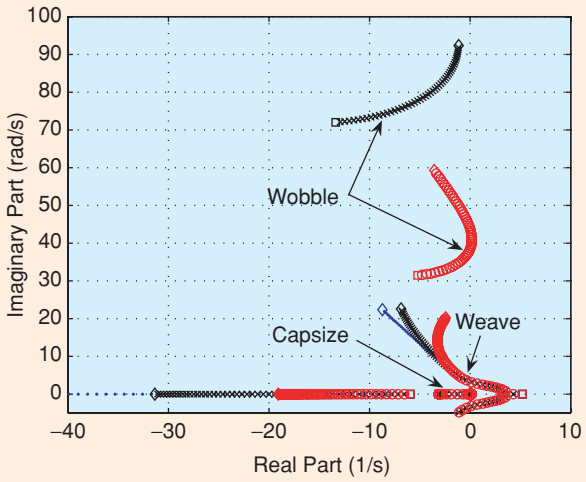

FIGURE 18 Root loci of the basic bicycle model with a flexible frame. The speed is varied from 0–20 m/s; the zero-speed end is represented by a square and the high-speed end by a diamond. The (blue) dotted loci correspond to the rigid frame, the (black) crosses to the high frame stiffness and damping values, and the (red) circles to the low stiffness and damping values.

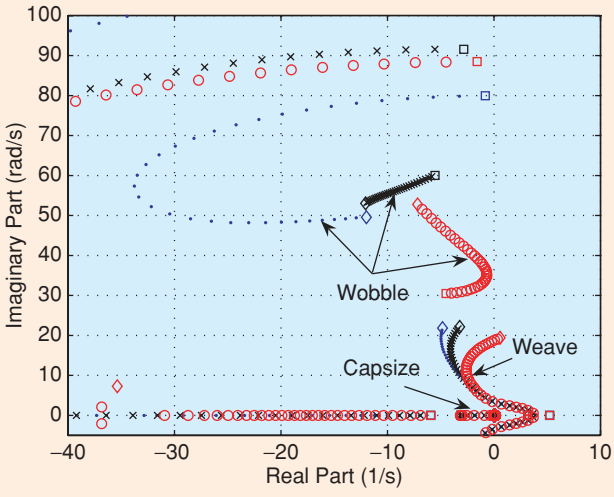

FIGURE 19 Root loci of the basic bicycle model with flexible frame and relaxed sideslipping tires. The speed is varied from 0–20 m/s; the zero-speed end is represented by a square and the high-speed end by a diamond. The (blue) dotted loci correspond to the rigid frame, the (black) crosses to the high frame stiffness and damping values, and the (red) circles to the low stiffness and damping values. The properties illustrated here for the limited speed range of the bicycle are remarkably similar to those of the motorcycle, with its extended speed capabilities.

Tommy Smith's Wobble

Tommy Smith was born in 1933. He started riding motorized bicycles at the age of 13 and was racing motorcycles professionally by the age of 17. In 1952, Tommy had the opportunity to ride a modified 650 cc Triumph Thunderbird at the Bonneville Salt Flats in Utah, United States. At that time, fuel (as opposed to gasoline) motorcycles used about 70% methanol and 30% nitro methane; crankcase explosions occurred when higher nitro percentages were tried. To further increase the motorcycle's engine power, the cylinder head was reversed, so that the intake ports were pointing forward to achieve a ram air effect. This engine configuration made it impossible to sit on the machine in a conventional manner. For this reason, the motorcycle was fitted with a plywood board for the rider to lie prone on. Leathers were heavy and uncomfortable and so Tommy rode the bike wearing a fiberglass helmet, goggles, tennis shoes (with socks), and a Speedo bathing suit (see Figure D).

On the first high-speed run, the machine produced an eerie "floating" sensation that was probably the result of a veneer of loose salt on the running track combined with a lightly loaded front wheel, resulting from the high speed and unusual riding position. Engine revolution and speed measurements taken at the time suggested that there was approximately 4.5 m/s of longitudinal tire-slip velocity. An accompanying lateral drifting phenomenon had to be corrected with small handlebar inputs that were required every 5–10 s. The need for continuous steering corrections may have also been associated with an unstable capsize mode with an unusually large growth rate and the lack of constraint between the rider and machine, both related to the riding position. Detailed calculations relevant to the situation described have not been carried out, so far as the authors are aware. The official one-way speed achieved was 147.78 mi/h, which was not to be exceeded by a 650-cc-motorcycle rider for another ten years.

On 25 August 1952, Tommy made his third high-speed run. Everything started normally—the floating sensation was the same as it had been on previous tests. Suddenly, the motorcycle went into a high-speed wobble and Tommy held tightly onto the handlebars to prevent himself from falling off. After a period of 3–5 s, the wobble was so violent that Tommy "hit the salt" and slid through the first 1/10 mi speed trap at an official speed of 139 mi/h. The speed of the motorcycle was not recorded! Although the motorcycle was only slightly damaged, Tommy's abrasion injuries were severe enough to keep him out of the Korean War. At the time, it was suggested that Tommy's light weight contributed to the motorcycle's instability, because heavier riders did not experience wobble at similar speeds. This suggestion that light riders might be prone to instability has been investigated by computer simulation studies [43]. The mobility of the rider relative to the motorcycle, as well as his rearward positioning, which led to a reduction in the front wheel load, are likely to have been important influences on the machine problem treated above.

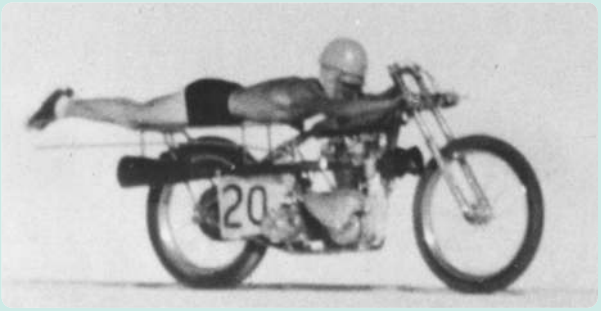

FIGURE D 24 Modified Triumph Thunderbird. Tommy Smith riding a modified 650-cc Triumph Thunderbird at the Bonneville Salt Flats in Utah. Note the forward-facing air intake ports.

increasingly less damped and possibly unstable at higher speeds. Wobble is a higher frequency (typically 7–9 Hz) motion that involves primarily the steering system. In contrast to the bicycle study presented in this article, [47] predicts that the wobble mode is well damped at low speeds, becoming lightly damped at high speeds.

In particular, the study shows that tire relaxation is an important contributor to the prediction of wobble and the quantitative characteristics of high-speed weave. The influences of parameter variations on the vehicle's dynamic behavior are also studied, and the results obtained are for the most part aligned with the behavior of vehicles of the time. Of particular importance is the predicted influence of the steering damper on the wobble-mode damping and the destabilizing effect that the damper has on the weave mode. The positive effect of moving the rear frame mass center forward, the critical impact on stability of the steering-head angle, the mechanical trail, and the front frame mass center offset from the steering axis are also demonstrated. A recurring theme is the need to find compromises under variations in these critical parameters.

Leaving briefly the constant-forward-speed case, [48] represents the first attempt to study the effects of acceleration and deceleration on the stability of motorcycles. A rather simple approach, in which the longitudinal equation of motion is decoupled from the lateral equations, gives the longitudinal acceleration as a parameter of the lateral motion. The acceleration parameter contributes to longitudinal inertia forces, which are included in standard stability computations. Such computations lead to some tentative conclusions, which depend on knowledge of the influence of loading on tire force and moment properties. More recent results [49], which are based on a higher fidelity model, are not supportive of the conclusions given in [48]. In [49], it is found that braking and acceleration have little influence on the frequency and damping of the weave mode. It is also

concluded in [49] that descending a hill or braking have a substantial destabilizing effect on the wobble mode. Conversely, the wobble-mode damping increases substantially under acceleration or ascending an incline, for small perturbations from straight running. An open issue is the influence of acceleration or braking on a cornering machine.

Tire Modeling

Modeling the generation of shear forces and moments by pneumatic tires has been approached in various ways, which recognize the physics of the situation in more or less detail. At one extreme, physical models [50]–[52] contain detailed descriptions of the tire structure and the tread-ground interactions, while, at the other, empirical formulas [50]–[53] come from fitting curves to measured data. In the middle ground, simple physical models provide good representations of the basic geometry and the distributed tire-ground rolling contact. The detailed models are effective in terms of accuracy and range of behavior covered but are computationally demanding to use. Contemporary high-fidelity models, which can be used over a wide variety of operating conditions, are almost exclusively of the empirical variety. An overview of many of these ideas in the context of car tires is given in [51].

The basis for contemporary tire models are magic formulas [51], [53]–[55], which are empirical models favored for their ability to accurately match tire force and moment data covering a full range of operating conditions. The original development was for car tires [56], in which context magic formula models are now dominant. These models describe the steady-state longitudinal forces, side forces, aligning moments, and overturning moments as functions of the longitudinal slip, sideslip, camber angle, and normal load. The extension of magic formula ideas to motorcycle tires is relatively recent, with substantial changes needed to accommodate the changed roles of sideslip and cambering in the force and moment generation process. When finding the parameters that populate the magic formulas, constraints must be placed on the parameter set to ensure that the tire behavior is reasonable under all operating conditions, some of which may be beyond those used in the parameter identification process. Although limited tire-parameter information can be found in the literature, models can be augmented with available experimental force and moment data. A full set of parameters for modern front and rear high-performance motorcycle tires can be found in [42]. Additional data are available in [51], [53]–[55], and [57]–[60].

Aerodynamic Forces

The importance of aerodynamic forces on the performance and stability of high-powered motorcycles at high speeds was demonstrated in [61]. Wind tunnel data were obtained for the steady-state aerodynamic forces acting on a wide range of motorcycle-rider configurations. It appears from the results in [61] that the effects of aerodynamic side forces, yawing moments, and rolling moments on the lateral stability of production motorcycles are minor. However, the drag, lift, and pitching moments contribute significantly to changes in the posture of the machine on its suspension and also to the tire loads. Aiming to explain the high-speed weave stability problem, [61] introduces these aerodynamic effects into the model of [47] using aerodynamic parameters corresponding to a streamlined machine. These results yield the conclusions that aerodynamic effects lead to only minor changes in the wobble mode and that high-speed weave difficulties cannot be attributed entirely to steady-state aerodynamic loading. As a result, it is postulated in [61] that the problem may involve nonsteady aerodynamic influences. To fully appreciate aerodynamic effects, it is necessary to employ a state-of-the-art model that includes the suspension system as well as tire models that recognize the influences of load changes. In such models [44], the aerodynamic drag and lift forces and the pitching moments are represented as being proportional to the square of the speed.

Structural Flexibility

Motivated by the known deterioration in the steering behavior resulting from torsional compliance between the wheels, [62] extends the model of [47] by allowing the rear wheel to camber relative to the rear frame. This freedom is constrained by a parallel spring-damper arrangement. It was found that swingarm flexibility had very little influence on the capsize and wobble modes, but it reduced the weave mode damping at medium and high speeds. The removal of the damping associated with the swingarm flexibility made no material difference to these findings. The results indicate that a swingarm stiffness of 12,000 N-m/rad for a high-performance machine would bring behavior approaching closely that for a rigid frame. Product development over the last 30 years has clearly involved substantial stiffening of the swingarm structure, such that most contemporary designs are probably deep into diminishing returns for additional stiffness.

Experimental work [63]–[66] shows that the theory existing at the time overpredicted the wobble-mode damping at moderate speeds, at which the damping is often quite small. In particular, [65] associates the low medium-speed-wobble damping with front fork compliance and shows improved behavior from stiffer forks. It is also shown in [65] that stiffening the rear frame with additional structures increased the damping of the weave mode.

The discrepancy between theory and experiment, mainly with respect to the damping of the wobble mode and its variation with speed, is substantially removed by the results of [40] and [41], where mathematical models were extended to include front frame compliances. In particular, [40] employs three model variants A, B, and C. The A model allows the front wheel to move laterally along the wheel spindle. The B model allows torsional compliance in the front frame about an axis parallel to the steer axis, while the C model allows twisting of the front frame relative to the rear frame about an axis perpendicular to the steering axis.

In each case, the new compliance involves a parallel spring-damper arrangement. The parameters from four different large production motorcycles are used. The following conclusions are drawn. 1) The torsional freedom parallel to the steering axis makes very little difference to the results obtained from the stiff-framed model. 2) The front-wheel lateral compliance results in a decrease in the wobble-mode damping, but the associated speed dependence is not supported by experiment. This flexibility also results in improved weave-mode damping at moderate speeds but worsens it for high speeds, which is where it matters. It is suggested that the lateral stiffness should be made large but that such stiffening brings diminishing returns beyond an intermediate stiffness level. 3) The C-model freedom leads to the prediction of the observed intermediate-speed low damping of the wobble mode, with higher damping at high speeds deriving from the frame compliance. Thus, the compliance may to some extent contribute to good behavior. In an independent study, [41] confirms the findings described above. Apart from varying the torsional stiffness, the effect of changing the height of the lateral fork bending joint was also examined. The analysis concluded that the lateral bending of the front fork should be reduced by stiffening and that the bending axis should be located as close to the pavement as possible. It also concluded that the "best" front-wheel suspension system should be designed to have high lateral stiffness without being excessively heavy.

Measured static torsional stiffness data for motorcycle frames are given in [58] and [67]–[69], while [68] and [69] also include the results of dynamic testing. Stiffnesses for large motorcycles from the past apparently lie in the range of 25,000–150,000 N-m/rad, where the influence on stability properties is marked. Predicting the wobble mode properly and understanding the need for a steering damper depend on accounting for frame torsional compliance in the steering-head region and lateral fork bending.

This frame flexibility work is consolidated in [70], where a motorcycle model is developed for straight-running studies with design parameters and tire properties obtained from laboratory experiments. The model constituents are, in addition to those given in the earlier model [47], lateral and frame twist flexibilities at the steering head, a flexibility of the rear wheel assembly about an inclined hinge, a roll freedom associated with the rider's upper body, in-plane aerodynamic effects, and more elaborate tire modeling. Hands-on and hands-off cases are presented, and the results are in agreement with empirical observations and experimental findings of [71]. The results show the advantage that can be derived in respect of the weave mode damping from a long wheelbase and a large steering-head angle. The model of [70] was subsequently rebuilt using a modern multibody simulation package [72], confirming the original. In the context of contemporary high-performance machines, the only frame flexibility deemed to be important is that associated with the steering head and front forks [42], [44].

Rider Modeling

In early motorcycle and bicycle models, the rider is considered to be no more than an inert mass rigidly attached to the rear frame [17], [47]. In [57] and [58], the rider's lower body is represented as an inert mass attached to the rear frame, while the upper body is represented as an inverted pendulum that has a single roll freedom constrained by a parallel spring-damper arrangement. The parameter values come from simple laboratory experiments, which show that values can vary significantly from rider to rider [73]. This single-degree-of-freedom inverted pendulum rider model is also used in [70].

The straight-running stability of a combined motorcycle rider model, which focuses on the frame flexibilities and the rider's dynamic characteristics, is studied in [73]. This 12-degree-of-freedom model includes two rider freedoms. The first is associated with the rolling motion of the rider's upper body, while the second allows the rider's lower body to translate laterally relative to the motorcycle's main frame. Both bodies associated with the rider are restored to their nominal positions by linear springs and dampers. The system parameters are found experimentally, and the rider data, in particular, is measured by means of forced vibration experiments, whereby the frequency responses from vehicle roll to rider body variables are obtained. The frequency and damping ratios of the wobble and weave modes are calculated at various speeds and compared with results obtained from experiments conducted with four motorcycles covering a range of sizes. A model without rider freedoms (a reduction of two degrees of freedom) is used for comparison. In general terms, there is very good agreement between the experimental results for each of the four machines and the detailed model, with a tendency for the measured damping factors to be a little greater than those predicted.

The effect of individual rider parameters on the rider-motorcycle system stability is also investigated analytically. It is found that the rider's vibration characteristics influence both wobble and weave. The parameters of the rider's upper body motion are most influential on weave, while those concerned with the rider's lower body primarily influence the wobble mode.

The role of the rider as an active controller is studied in some detail in [74], where it is recognized that inadvertent rider motions can have a significant influence on the vehicle's behavior. The focus of [74] is to treat the rider as a feedback compensator that maps the vehicle's roll angle errors into a steering torque, where the controller's characteristics are chosen to mimic those of the rider's neuromuscular system. The rider is modeled (roughly) as being able to control his upper body roll angle as well as the steering torque; the steering torque influence is found to be dominant.

A motorcycle rider model similar to that studied in [73] is investigated in [75] to find those aspects of the rider's control action that are most important in the description of single-lane-change maneuvering behavior. In this case, the rider

model comprises upper and lower body masses that are both free to roll relative to the motorcycle's main frame. The rider is assumed to generate three control torques that are applied to the steering system from the rider upper body, the upper body from the lower body, and the lower body from the rear frame. The rider representation, which plays the role of a feedback controller tasked with tracking a heading, is as a proportional controller. Simulations for a single-lane-change maneuver are compared with measurements generated by 12 different riders. The results show that, for a running speed of 17 m/s, a good match can be obtained between the simulation model with suitably chosen controller parameters and the measured responses of the different riders. The results also suggest that the most important control input is the steering torque. While it is possible to control the motorcycle with lower body lean movement, much larger torques are required in this case. Normally, lower body control is utilized to assist steering torque control, while the upper body is controlled only to keep the rider in the comfortable upright position.

A complex rider model that comprises 12 rigid bodies representing the upper and lower body, the upper and lower arms, and the upper and lower legs, with appropriate mass and inertia properties is introduced in [76]. The various rider model masses are restrained by linear springs and dampers so that rider motions such as steering, rolling, pitching, weight shifting and knee gripping are possible. Rider control actions associated with these degrees of freedom are also modeled using proportional control elements. Steady-state cornering and lane-changing maneuvers are studied.

Suspension and Cornering Models

Under steady-state cornering it is clear that a motorcycle's forward speed, yaw rate, lateral acceleration, and lean angle are constant, while the suspension posture of the machine, the tire force system, and the aerodynamic forces are all functions of the lean angle. Essential components of high-fidelity cornering models include [44]: 1) a rigid rear frame, which has six degrees of freedom; 2) a front frame joined to the rear frame using an inclined steering system with a compliance included between the steering head and the rear frame; 3) spinning road wheels, which include thick profiled tire descriptions, where the dynamic migration of the road-tire ground contact point under cornering is modeled; 4) an elaborate tire force and moment representation informed by extensive measurements; 5) lag mechanisms by which tire forces are delayed with respect to the slip phenomena that produce them; 6) aerodynamic effects, which allow the tire loads and machine posture to be properly represented under speed variations; 7) a realistic suspension model; and 8) the freedom for the rider's upper body to roll relative to the rear frame of the vehicle. The accuracy of predicted behavior depends not only on effective conceptual modeling and multibody analysis but also on good parameter values.

The in-plane modes present under straight-running conditions are shown in Figure 20; similar plots can be found in [44]. The in-plane modes that are associated with the suspension and tire flexibilities are referred to as the front suspension pitch mode, the rear suspension pitch mode, the front wheel-hop mode, and the rear wheel-hop mode. These modes are insensitive to speed variations and are decoupled from the out-of-plane modes described above.

The cornering situation is considerably more complex than the straight-running case, since the in-plane and out-of-plane motions are coupled and these interactions tend to increase with roll angle. As a consequence, several straight-running modes merge together to form combined cornering modes with the particular characteristics shown in the right-

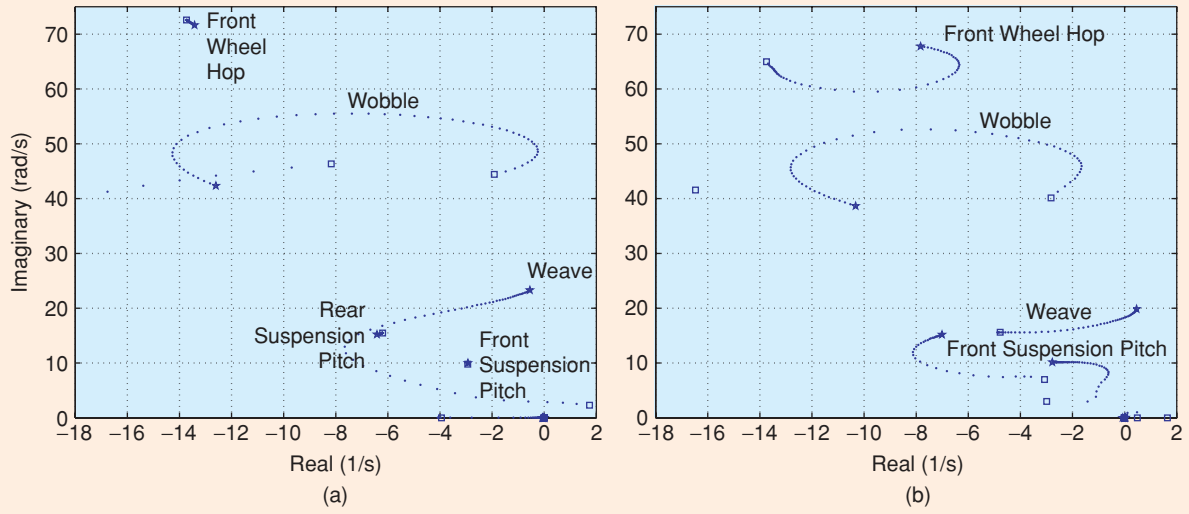

FIGURE 20 Motorcycle root locus plots: (a) straight-running and (b) 30° of roll angle with speed the varied parameter. The speed is increased from (a) 5 m/s (□), (b) 6 m/s (□) to 60 m/s (⋆).

hand root locus plot in Figure 20. Cornering weave is similar in frequency to straight-running weave at high speeds, but for the machine studied here, the weave-mode damping decreases as the lean angle increases. The suspension system contributes significantly to the machine characteristics, as observed experimentally. The influence of suspension damping on the weave mode is demonstrated both analytically and experimentally in [66] and [77]. Under cornering, the wobble mode involves suspension movement, and the previously speed-independent suspension-pitch and wheel-hop modes now vary markedly with speed. An interaction between the front wheel-hop and wobble modes occurs when the two modes are close enough in terms of natural frequency. This interaction is possibly linked to wheel patter, which is known anecdotally [78]. The coupling of the in-plane and out-of-plane motions also suggests the possibility of road excitation signals being transmitted into the lateral motions of the vehicle, causing steering oscillations [43].

The early literature [77] discusses the existence of a modified weave mode that occurs under cornering conditions, where the suspension system plays an important role in its initiation and maintenance. To investigate the effect of suspension damping on cornering weave, [77] benchmarks several front and rear suspension dampers in laboratory experiments and riding tests. Motorcycle stability is found to be sensitive to suspension damping characteristics, while cornering weave instability is to some extent controllable through rear suspension damper settings. As stated in [77], "... slight road surface undulations exacerbate the problem, which is generally confined to speeds above 60 mph and roll angles in excess of 25 deg from pavement-perpendicular ...". It is also found that, as the speed is increased, cornering weave is produced at smaller roll angles. A separate study [79] demonstrates, using a simple analysis, the possibility of interaction between pitch and weave modes at high speeds, where the lightly damped weave-mode natural frequency approaches that of the pitch mode. Although for straight running the coupling of in-plane and out-of plane motions is weak, for steady-state cornering the coupling between the two modes increases with increased roll angle, indicating that the inclusion of pitch and bounce freedoms in motorcycle models is essential for handling studies involving cornering.

Cornering experiments described in [66] quantify the influences of various motorcycle design parameters and operating conditions on wobble and weave. Tests with a range of motorcycles and riders are carried out for both straight running and steady-state cornering. The wobble mode, which is excited by a steering torque pulse input from the rider, is seen to be self-sustained during hands-off straight running at a moderate speed of 18 m/s; the measured wobble frequency is 5.4 Hz, which is lower than the theoretical prediction. More importantly, under steady-state cornering, measurements of cornering weave responses at 27 m/s, involving oscillations in the suspension system, indicate a frequency of 2.2 Hz, while at 36 m/s the frequency is 2.6 Hz. It is also found that the weave oscillations die out once the rider reduces the roll angle. Further, [66] also demonstrates that reduced rear suspension damping, increased rear loading, and increased speed increases the tendency for the motorcycle to weave. As predicted by theory, the frequency of wobble varies little with speed, while that of weave increases with speed.

Significant steps in the theoretical analysis of motorcycle behavior are documented in [57] and [58]. The model developed considers small perturbations about straight-running conditions but also for the first time about steady-cornering conditions. The model in [57] is used to calculate the eigenvalues of the small-perturbation linearized motorcycle, where the results for straight running are consistent with the conventional wisdom. The way the weave- and wobble-mode characteristics are predicted as varying with speed is conventional, with new front- and rear-suspension pitch and wheel-hop modes almost independent of speed appearing. Under cornering conditions, the interaction of these otherwise uncoupled modes produces more complicated modal motions. The cornering weave and combined wheel-hop/wobble modes are illustrated, and root loci are plotted to observe the sensitivity of the results to parameter variations. Surprisingly, it is predicted that removing the suspension dampers hardly affects the stability of the cornering weave mode, contrary to the experiences of [66] and [77].

One of the original aims of [44] is to investigate the apparent conflict between the results of [80] on the negligible influence of suspension damping on the stability of cornering weave and the anecdotal and experimental evidence of [66] and [77]. Cornering root loci with the rear suspension damping varied are reproduced and the damping is found to have a significant influence, indicating a probable error in the calculations in [80]. The model presented in [44] is enhanced in [42] to include magic formula tire models with the additional features included in [81].

The influence of the front suspension system on the ride qualities of a motorcycle is studied in [82]. A typical suspension unit is modeled on the basis of its inner structure and functionality, which give rise to the spring forces, viscous damping forces, friction forces, and oil lock forces. Sine-wave excitation experiments show that the model represents the unit accurately. Further experiments are conducted, this time to check the validity of the fork unit model combined with a simplified motorcycle model that comprises the vertical and longitudinal dynamics. The results obtained for riding over bumps and under braking agree with measurements. The influence of the suspension characteristics on riding qualities of the vehicle are found by simulation; experiments verify the findings.

Experimental cornering results obtained from an instrumented motorcycle are presented in [83]. The motorcycle is fitted with steering torque and angle transducers. Fiber-optic gyros are used to measure the roll rate and yaw rate, and strain gauges provide tire force and moment data.

This paper provides experimental data that are used for model qualification.

A study of the effects of road profiling on motorcycle steering responses is presented in [43]. The results show that under cornering conditions, regular low-amplitude road undulations that would not trouble four-wheeled vehicles can be a source of considerable difficulty to motorcycle riders. At low machine speeds, the wobble and front suspension pitch modes are likely to respond vigorously to resonant vertical-displacement road forcing, while, at higher speeds, the weave and front wheel-hop modes may be similarly affected. Connections between resonant responses and a class of single-vehicle loss-of-rider-control accidents are postulated. This work has several practical consequences. First, these results appear to explain the key features of many stability-related road traffic accidents reported in the popular literature and help to show why motorcycles that behave perfectly well for long periods can suddenly suffer serious and dangerous oscillation problems. Such oscillations are likely to be difficult to reproduce and study experimentally. Second, road builders and maintainers, as well as motorcycle manufacturers, should be aware of the possibility of strong resonant responses to small but regular undulations under certain critical running conditions. These conditions are characterized by the machine speed, the lean angle, the rider's mass and posture, and the road profile wavelength.

CONCLUSIONS

Research and scholarship relating to single-track vehicles involves, to a large extent, two separate communities that can benefit from a higher level of interaction. One group favors the use of simple bicycle models, while the other is concerned with high-performance motorcycles and the development of models with a high level of quantitative predictive capability over a wide operating envelope.

The simple models can be regarded as derivatives or simplifications of Whipple's model. In these models, the lateral motion constraints at the road contact are nonholonomic and thus special techniques may be needed to form correct equations of motion. When the tire is regarded as constraining the motion of the vehicle, the model validity is restricted to low speeds (<10 m/s), low frequencies (<1.0 Hz), and low tire-force utilization associated with benign maneuvering ($<20\%$ of capacity).

The model of Timoshenko and Young [29] represents the lowest level of complexity of any potential usefulness; their model has no rake, no trail, no inertias, no front frame mass, and a point-mass representation of the rear frame. The Timoshenko-Young model leads one to conclude that the steer angle and speed completely determine the lateral motion of the base point of an inverted pendulum that represents the vehicle's roll dynamics. In terms of understanding single-track vehicle steering, this level of modeling complexity is too low, since unrealistic steer angle control must be accommodated. The self-steering influences, which are vital to the operation of a real single-track vehicle, are completely absent. Nevertheless, steer-displacement control inputs that allow a prescribed path to be followed while the rolling motion is properly stabilized have been optimized on simple Timoshenko-Young-type models and applied to sophisticated machine models with some success.

Whipple's model, when linearized for constant-speed straight running, yields two second-order equations of motion in rolling and steering. The Whipple model, while simple enough for control system optimization studies, contains a sufficient level of physical realism to make it credible. Physical influences deriving from the vehicle's design can be seen to combine in complex ways to give an effective steering inertia, steering damping, and steering stiffness. The Whipple model also provides an appreciation of the complex interactions between the roll angle, roll velocity, and roll acceleration, and the steering torque. Linear versions of Whipple-type models are useful for explaining nonminimum phase responses, the benefits of feedback, and achievable robustness margins in single-track vehicles.

In models of the Timoshenko-Young type, the roll dynamics are driven kinematically by the steer angle, the steer velocity, the steer acceleration, and the vehicle acceleration inputs. The advantage of these models is that considerable insight into the stability and steering control of single-track vehicles, within the model applicability boundaries, can be gained from their separable design parameter influences. Although such insights cannot easily be developed by referring to the numerical results derived from more complex models, comprehensive models surely have their place in enabling effective virtual product design and testing across the full operating envelope. The essential features of modern motorcycle design models include: 1) multiple rigid bodies and a complex set of allowed motion freedoms; 2) detailed tire force and moment models, incorporating static behavior up to and possibly beyond the tire saturation limits, as well as transient behavior; 3) case-dependent frame and rider compliances; 4) suspension systems; 5) aerodynamic forces and moments; and 6) detailed geometric models for accurately describing all of the external forces. When motorcycles are ridden "on the limit," the stability and performance of the machine are restricted by the properties of the tires, the suspension setup, the weight distribution, the frame stiffness properties, and the steering damping. A practical virtual design and testing facility must be able to accurately predict every feature of this limit behavior.

In relation to trajectory tracking on the boundaries of the vehicle's capability—essentially the racing problem—it is clear that performance is limited by tire force saturation and transient dynamics, among other things. It appears to be a considerable act of faith to regard the ultimate performance as calculable on the basis of nonholonomic rolling constraints! In the future, we hope to see more elaborate models, of the motorcycle-fraternity type, applied to minimum lap time and optimal-trajectory tracking problems.

Complexity-related difficulties, implicit in comprehensive motorcycle modeling activities, are an exciting opportunity, rather than a threat to be feared and avoided. Indeed, the thoughtful use of powerful multibody modeling tools makes routine the study of problems that would have been deemed intractable only a decade ago. The challenges facing modelers include a systematic approach to removing redundancy in nonlinear models and the retention of key insights, which tend to be obscured or even destroyed, in model reduction exercises. The challenges facing control theorists include: 1) the development of general theories for reducing complex nonlinear models that guarantee the reduced-order model's dynamic fidelity; 2) removing assumptions that currently make general control theories inapplicable to nonlinear mechanics problems, and 3) the parallel development of computational platforms that support complex controller synthesis applications.

ACKNOWLEDGMENTS

The authors would like to thank Prof. Karl Åström, Prof. Malcolm Smith, and the reviewers for their helpful suggestions.

AUTHOR INFORMATION

David J.N. Limebeer (d.limebeer@imperial.ac) received the B.Sc. degree in electrical engineering from the University of Witwatersrand, Johannesburg, in 1974, the M.Sc. and Ph.D. degrees in electrical engineering from the University of Natal, Durban, South Africa, in 1977 and 1980, respectively, and the D.Sc. degree from the University of London in 1992. He has been with Imperial College London since 1984, where he is currently the head of the Department of Electrical and Electronic Engineering. He has published over 100 papers and a textbook on robust control theory. Three of his papers have been awarded prizes, including the 1983 O. Hugo Schuck Award. He is a past editor of *Automatica* and a past associate editor of *Systems and Control Letters* and the *International Journal of Robust and Nonlinear Control*. He is a Fellow of the IEEE, the IEE, the Royal Academy of Engineering, and the City and Guilds Institute. His research interests include control system design, frequency response methods, H-infinity optimization and mechanical systems. He is qualified as an IAM senior motorcycle instructor and received a RoSPA certificate for advanced motorcycling. He can be contacted at Imperial College London, Department of Electrical and Electronic Engineering, Exhibition Road, London SW7 2AZ U.K.

Robin S. Sharp is a professorial research fellow in the Department of Electrical and Electronic Engineering at Imperial College London. He is a member of the Dynamical Systems and Mechatronics Working Group of the International Union of Theoretical and Applied Mechanics, the editorial board of *Vehicle System Dynamics,* and the editorial advisory board of *Multibody System Dynamics*. He was first vice-president and secretary general of the International Association for Vehicle System Dynamics, editorial panel member and book review editor for *The Proceedings of the Institution of Mechanical Engineers, Journal of Mechanical Engineering Science, Part C*, and editorial panel member of *The Proceedings of the Institution of Mechanical Engineers, Part D, Journal of Automobile Engineering*. From 1990–2002, he was professor of automotive product engineering at Cranfield University. He was a visiting associate research scientist at the University of Michigan Transportation Research Institute, Ann Arbor. His research covers topics in automotive dynamics and control and in control and stability of single-track vehicles, unmanned air vehicles, and the application of optimal preview and learning control to road vehicle driving/riding.

REFERENCES

[1] A. Sharp, *Bicycles and Tricycles: An Elementary Treatise on Their Design and Construction*. White Plains, NY: Longman, 1896. (Reprinted as: *Bicycles and Tricycles: A Classic Treatise on Their Design and Construction*. Mineola, NY: Dover, 1977.)

[2] D.V. Herlihy, *Bicycle: The History*. New Haven, CT: Yale Univ. Press, 2004.

[3] M. Hamer, "Brimstone and bicycles," *New Scientist*, issue 2428, pp. 48–49, Jan. 2005.

[4] N. Clayton, *Early Bicycles.* Princes Risborough, Bucks, UK: Shire Publications, 1986.

[5] F.J. Berto, *The Dancing Chain: History and Development of the Derailleur Bicycle*. San Francisco, CA: Van der Plas Publications, 2005.

[6] "The Bicycle Museum of America" [Online]. Available: http://www.bicyclemuseum.com/

[7] "Pedaling history bicycle museum" [Online]. Available: http://www.pedalinghistory.com/

[8] "Metz bicycle museum" [Online]. Available: http://www.metzbicyclemuseum.com/

[9] "Canada science and technology museum" [Online]. Available: http://www.sciencetech.technomuses.ca/

[10] "Canberra bicycle museum" [Online]. Available: http://canberrabicyclemuseum.com.au/

[11] "National motorcycle museum" [Online]. Available: http://www.nationalmcmuseum.org/

[12] "London motorcycle museum" [Online]. Available: http://www.motorcycle-uk.com/lmm/beginning.html

[13] "Allen vintage motorcycle museum" [Online]. Available: http://www.allenmuseum.com/

[14] "Sammy Miller museum" [Online]. Available: http://motorcycle.com/mo/mcfrank/sammymuseum.html

[15] "Motorcycle hall of fame museum" [Online]. Available: http://home.ama-cycle.org/

[16] W.J.M. Rankine, "On the dynamical principles of the motion of velocipedes," *The Engineer*, pp. 2, 79, 129, 153, 175, 1869/1870.

[17] F.J.W. Whipple, "The stability of the motion of a bicycle," *Q. J. Pure Appl. Math.*, vol. 30, pp. 312–348, 1899.

[18] H. Goldstein, *Classical Mechanics*, 2nd ed. Reading, MA: Addison-Wesley, 1980.

[19] M.E. Carvallo, "Théorie du movement du monocycle, part 2: Théorie de la bicyclette," *J. L'Ecole Polytechnique,* vol. 6, pp. 1–118, 1901.

[20] F. Klein and A. Sommerfeld, *Über die Theorie des Kreisels*. Teubner, Leipzig, 1910, Chap. IX, Sec. 8, "Stabilität des Fahrrads," Leipzig, Germany: B.G. Teubner, pp. 863–884.

[21] D.E.H. Jones, "The stability of the bicycle," *Phys. Today*, vol. 23, no. 4, pp. 34–40, 1970.

[22] R.D. Roland, "Computer simulation of bicycle dynamics," in *Proc. ASME Symp. Mechanics Sport*, 1973, pp. 35–83.

[23] E. Döhring, "Stability of single-track vehicles," *Institut für Fahrzeugtechnik, Technische Hochschule Braunschweig, Forschung Ing.-Wes.*, vol. 21, no. 2, pp. 50–62, 1955.

[24] J.I. Neĭmark and N.A. Fufaev, "Dynamics of nonholonomic systems," (Amer. Math. Soc. Translations Math. Monographs, vol. 33), 1972.

[25] R.S. Hand, "Comparisons and stability analysis of linearized equations of motion for a basic bicycle model," M.Sc. Thesis, Cornell Univ., 1988.

[26] A.L. Schwab, J.P. Meijaard, and J.M. Papadopoulos, "Benchmark results on the linearized equations of motion of an uncontrolled bicycle," in *Proc. 2nd Asian Conf. Multibody Dynamics*, Aug. 2004, pp. 1–9.

[27] K.J. Åström, R.E. Klein, and A. Lennartsson, "Bicycle dynamics and control," *IEEE Control Syst. Mag.*, vol. 25, no. 4, pp. 26–47, 2005.

[28] R.E. Klein, "Using bicycles to teach system dynamics," *IEEE Control Syst. Mag.*, vol. 6, no. 4, pp. 4–9, 1989.
[29] S. Timoshenko and D.H. Young, *Advanced Dynamics*. New York: McGraw-Hill, 1948.
[30] A.M. Letov, *Stability in Nonlinear Control Systems*. Princeton, NJ: Princeton Univ. Press, 1961.
[31] N.H. Getz, "Control of balance for a nonlinear nonholonomic nonminimum phase model of a bicycle," in *Proc. American Control Conf.*, 1994, pp. 148–151.
[32] N.H. Getz and J.E. Marsden, "Control of an autonomous bicycle," in *Proc. IEEE Conf. Robotics Automation*, 1995, pp. 1397–1402.
[33] J. Hauser, A. Saccon, and R. Frezza, "Achievable motorcycle trajectories," in *Proc. 43rd CDC*, Paradise Island, Bahamas, 14–17 Dec. 2004, pp. 3944–3949.
[34] K.J. Åström, "Limitations on control system performance," *Euro. J. Control*, vol. 6, no. 1, pp. 2–20, 1980.
[35] Anon., *Autosim 2.5+ Reference Manual*. Mech. Simulation Corp., Ann Arbor MI, 1998 [Online]. Available: http://www.carsim.com
[36] A.L. Schwab, J.P. Meijaard, and J.D.G. Kooijman, "Experimental validation of a model of an uncontrolled bicycle," in *Proc. III European Conf. Computational Mechanics: Solids, Structures Coupled Problems Engineering*, Lisbon, Portugal, 5-9 June 2006, paper 98.
[37] R.A. Wilson-Jones, "Steering and stability of single-track vehicles," in *Proc. Auto. Div. Institution Mechanical Engineers*, 1951, pp. 191–199.
[38] A.L. Schwab, J.P. Meijaard, and J. M. Papadopoulos, "A multibody dynamics benchmark on the equations of motion of an uncontrolled bicycle," in *Proc. ENOC-2005*, Eindhoven, The Netherlands Aug. 2005, pp. 1–11.
[39] J. Fajans, "Steering in bicycles and motorcycles," *Amer. J. Phys.*, vol. 68, no. 7, pp. 654–659, 2000.
[40] R.S. Sharp and C.J. Alstead, "The influence of structural flexibilities on the straight running stability of motorcycles," *Vehicle Syst. Dyn.*, vol. 9, no. 6, pp. 327–357, 1980.
[41] P.T.J. Spierings, "The effects of lateral front fork flexibility on the vibrational modes of straight-running single-track vehicles," *Vehicle Syst. Dyn.*, vol. 10, no. 1, pp. 21–35, 1981.
[42] R.S. Sharp, S. Evangelou, and D.J.N. Limebeer, "Advances in the modelling of motorcycle dynamics," *Multibody Syst. Dyn.*, vol. 12, no. 3, pp. 251–283, 2004.
[43] D.J.N. Limebeer, R.S. Sharp, and S. Evangelou, "Motorcycle steering oscillations due to road profiling," *J. Appl. Mech.*, vol. 69, no. 6, pp. 724–739, 2002.
[44] R. S. Sharp and D.J.N. Limebeer, "A motorcycle model for stability and control analysis," *Multibody Syst. Dyn.*, vol. 6, no. 2, pp. 123–142, 2001.
[45] V. Cossalter and R. Lot, "A motorcycle multi-body model for real time simulations based on the natural coordinates approach," *Vehicle Syst. Dyn.*, vol. 37, no. 6, pp. 423–447, 2002.
[46] R.S. Sharp, "The lateral dynamics of motorcycles and bicycles," *Vehicle Syst. Dyn.*, vol. 14, no. 6, pp. 265–283, 1985.
[47] R.S. Sharp, "The stability and control of motorcycles," *J. Mech. Eng. Sci.*, vol. 13, no. 5, pp. 316–329, 1971.
[48] R.S. Sharp, "The stability of motorcycles in acceleration and deceleration," in *Proc. Inst. Mech. Eng. Conf. Braking Road Vehicles*, London: MEP, 1976, pp. 45–50.
[49] D.J.N. Limebeer, R.S. Sharp, and S. Evangelou, "The stability of motorcycles under acceleration and braking," *J. Mech. Eng. Sci.*, vol. 215, no. 9, pp. 1095–1109, 2001.
[50] H.B. Pacejka and R.S. Sharp, "Shear force development by pneumatic tyres in steady state conditions: A review of modelling aspects," *Vehicle Syst. Dyn.*, vol. 20, no. 3–4, pp. 121–176, 1991.
[51] H.B. Pacejka, *Tyre and Vehicle Dynamics*. Oxford, U.K.: Butterworth Heinemann, 2002.
[52] S.K. Clark, Ed., *Mechanics of Pneumatic Tires*, 2nd ed. Washington DC: NTIS, 1981.
[53] E.J.H. de Vries and H.B. Pacejka, "Motorcycle tyre measurements and models," *Vehicle Syst. Dyn.*, vol. 29, pp. 280–298, 1998.
[54] E.J.H. de Vries and H.B. Pacejka, "The effect of tyre modeling on the stability analysis of a motorcycle," in *Proc. AVEC'98*, Nagoya, Soc. Automotive Engineers paper Japan, 1998, pp. 355–360.
[55] Y. Tezuka, H. Ishii, and S. Kiyota, "Application of the magic formula tire model to motorcycle maneuverability analysis," *J. Soc. Auto. Eng. paper Rev.*, vol. 22, no. 3, pp. 305–310, 2001.
[56] E. Bakker, L. Nyborg, and H.B. Pacejka, "Tyre modelling for use in vehicle dynamics studies," *Soc. Auto. Eng.*, paper 870421, 1987.
[57] C. Koenen and H.B. Pacejka, "Vibrational modes of motorcycles in curves," in *Proc. Int. Motorcycle Safety Conf.*, Washington, Motorcycle Safety Foundation, 1980, vol. II, pp. 501–543.
[58] C. Koenen and H.B. Pacejka, "The influence of frame elasticity, simple rider body dynamics, and tyre moments on free vibrations of motorcycles in curves," in *Proc. 7th IAVSD Symp. Dynamics Vehicles Roads Railway Tracks*, Cambridge, 1981, pp. 53–65.
[59] V. Cossalter, A. Doria, R. Lot, N. Ruffo, and M. Salvador, "Dynamic properties of motorcycle and scooter tires: Measurement and comparison," *Vehicle Syst. Dyn.*, vol. 39, no. 5, pp. 329–352, 2003.
[60] H. Sakai, O. Kanaya, and H. Iijima, "Effect of main factors on dynamic properties of motorcycle tires," *Soc. Auto. Eng.*, paper 790259, 1979.
[61] K.R. Cooper, "The effects of aerodynamics on the performance and stability of high speed motorcycles," in *Proc. 2nd AIAA Symp. Aerodynamics Sport Competition Automobiles*, Los Angeles, 1974.
[62] R.S. Sharp, "The influence of frame flexibility on the lateral stability of motorcycles," *J. Mech. Eng. Sci.*, vol. 16, no. 2, pp. 117–120, 1974.
[63] D.J. Eaton, "Lateral dynamics of the uncontrolled motorcycle," in *Proc. 2nd Int. Congr. Automotive Safety*, San Fransisco, 1973.
[64] M.K. Verma, R.A. Scott, and L. Segel, "Effect of frame compliance on the lateral dynamics of motorcycles," *Vehicle Syst. Dyn.*, vol. 9, no. 3, pp. 181–206, 1980.
[65] G.E. Roe and T.E. Thorpe, "A solution of the low-speed wheel flutter instability in motorcycles," *J. Mech. Eng. Sci.*, vol. 18, no. 2, pp. 57–65, 1976.
[66] D.H. Weir and J.W. Zellner, "Experimental investigation of the transient behaviour of motorcycles," *Soc. Auto. Eng.*, paper 790266, 1979.
[67] A. Clerx, "Stijfheid en sterkte van motorfietsframes," Dept. Mech. Eng., Tech. Univ. Eindhoven, Tech. Rep., 1977.
[68] C.G. Giles and R.S. Sharp, "Static and dynamic stiffness and deflection mode measurements on a motorcycle, with particular reference to steering behaviour," in *Proc. Inst. Mech. Eng./MIRA Conf. Road Vehicle Handling*, London, 1983, pp. 185–192.
[69] M.P.M. Bocciolone, F. Cheli, and R. Vigano, "Static and dynamic properties of a motorcycle frame: Experimental and numerical approach," Dept. Mech. Eng., Politecnico di Milano, Tech. Rep., 2005.
[70] R.S. Sharp, "Vibrational modes of motorcycles and their design parameter sensitivities," in *Proc. Int Conf. Vehicle NVH Refinement*, Birmingham, 3–5 May 1994, pp. 107–121.
[71] B. Bayer, "Flattern und pendeln bei krafträdern," *Automobil Industrie*, vol. 2, pp. 193–197, 1988.
[72] S. Evangelou and D.J.N. Limebeer, "Lisp programming of the 'sharp 1994' motorcycle model," 2000 [Online]. Available: http://www.ee.ic.ac.uk/control/motorcycles
[73] T. Nishimi, A. Aoki, and T. Katayama, "Analysis of straight running stability of motorcycles," in *Proc. 10th Int. Technical Conf. Experimental Safety Vehicles*, Oxford, 1–5 July 1985, pp. 1080–1094.
[74] D.H. Weir and J.W. Zellner, "Lateral-directional motorcycle dynamics and rider control," *Soc. Auto. Eng.* paper 780304, pp. 7-31, 1978.
[75] T. Katayama, A. Aoki, and T. Nishimi, "Control behaviour of motorcycle riders," *Vehicle Syst. Dyn.*, vol. 17, no. 4, pp. 211–229, 1988.
[76] H. Imaizumi, T. Fujioka, and M. Omae, "Rider model by use of multibody dynamics analysis," *Japanese Soc. Auto. Eng.*, vol. 17, no. 1, pp. 75–77, 1996.
[77] G. Jennings, "A study of motorcycle suspension damping characteristics," *Soc. Auto. Eng.*, paper *740628*, 1974.
[78] R.S. Sharp and C.G. Giles, "Motorcycle front wheel patter in heavy braking," in *Proc. 8th IAVSD Symp. Dynamics Vehicles Roads Railway Tracks*, Boston, 1983, pp. 578–590.
[79] R.S. Sharp, "The influence of the suspension system on motorcycle weave-mode oscillations," *Vehicle Syst. Dyn.*, vol. 5, no. 3, pp. 147–154, 1976.
[80] C. Koenen, "The dynamic behaviour of motorcycles when running straight ahead and when cornering," Ph.D. dissertation, Delft Univ. Technol., 1983.
[81] R.S. Sharp, D.J.N. Limebeer, and M. Gani, "A motorcycle model for stability and control analysis," in *Proc. Euromech Colloquium 404, Advances Computational Multibody Dynamics*, 1999, pp. 287–312.
[82] T. Kamioka, N. Yoshimura, and S. Sato, "Influence of the front fork on the movement of a motorcycle," in *Proc. SETC'97*, Yokohama, 1997, pp. 397–403.
[83] H. Ishii and Y. Tezuka, "Considerations of turning performance for motorcycles," in *Proc. SETC'97*, Yokohama, 1997, pp. 383–389.
[84] A. Hill, "Smith's prizes: award," *Cambridge Univ. Reporter*, p. 1027, 1899.
[85] D.G. Wilson, *Bicycling Science*. Cambridge, MA: MIT Press, 2004.
[86] C. Juden, "Shimmy," *Cycletouring*, pp. 208–209, June/July 1988.
[87] R.S. Sharp and D.J.N. Limebeer, "On steering wobble oscillations of motorcycles," *J. Mech. Eng. Sci.*, vol. 218, no. 12, pp. 1449–1456, 2004.
[88] T. Wakabayashi and K. Sakai, "Development of electronically controlled hydraulic rotary steering damper for motorcycles," in *Proc. Int. Motorcycle Safety Conf.*, Munich, 2004, pp. 1–22.
[89] J.P. Den Hartog, *Mechanical Vibration*. New York: Dover, 1985.
[90] P. Bandel and C. Di Bernardo, "A test for measuring transient characteristics of tires," *Tire Sci. Technol.*, vol. 17, no. 2, pp. 126–137, 1989.